Prathamesh Halagi

Characterization and Modelling of Lithium-ion batteries for Grid Applications

School of Technology and Innovations

Master's Thesis in Smart Energy

Vaasa 2021

ACKNOWLEDGEMENTS

I would like to express my gratitude to my supervisor, Prof. Hannu Laaksonen, who gave me this opportunity to pursue this Master's Thesis and for his precious advice, guidance and support throughout this project. It is a true honour to be associated with him.

I would like to take this opportunity to thank my co-supervisor, Chethan Parthasarathy, PhD, for introducing me to this exciting field of Research and for his constant support, valuable suggestions. Throughout this thesis, he has always been there and patiently responded without hesitation to all my queries.

I would also like to express my sincerest thanks to Prof. Rayko Toshev, who helped me at critical times with practical matters and laboratory works.

A special thanks to the School of Technology and Innovations, Electrical Engineering, University of Vaasa, Finland, without which the project would not have been possible

Finally, I would like to express my deepest gratitude to my parents, Mr Prasanna Halagi and Mrs Dnyanada Halagi, for their love and support throughout my studies. A special credit to my sibling Ms Pratiksha Halagi, my girlfriend, Ms Jaai Nasikkar and my friends for their continuous support and encouragement throughout my M.Sc. Studies.

UNIVERSITY OF VAASA
School of Innovations and Technology
Author: Prathamesh Halagi
Title of the Thesis: Characterization and Modelling of Lithium-ion Batteries for Grid Applications
Degree: Master of Science in Smart Energy
Programme: Smart Energy
Supervisor: Hannu Laaksonen
Co-Supervisor: Chethan Parthasarathy
Year: 2021 **Pages:** 91

ABSTRACT:

The demand for energy has been increasing, raising concerns about greenhouse gases and depleting renewable energy sources. This has made the use of renewable energy sources more evident in various applications. These renewable energy sources are recognized for their potential to reduce global warming and climate change. The use of smart grids will help in the reduction of these GHS's and CO_2 emissions. These grid applications necessitate energy storage systems in order to achieve smooth operation. Thus, Energy storage systems have become an essential technology for various applications such as land-based grid applications and Lithium-ion batteries will play a significant role.

Lithium-ion batteries have seen considerable development in the last couple of decades to enhance battery characteristics based on its safety, voltage/current capacities, operating temperatures, ageing, etc. Similarly, Lithium titanate oxide (LTO) battery cells have seen significant development as it is regarded to play a vital role in energy storage systems for large scale stationary grid applications. These batteries use LTO as active anode material instead of the traditional graphite. LTO batteries are recognised for various competencies ranging from higher safety margins, high thermal stability, low self-discharge rate and superior cycle performance. LTO batteries are relatively new, and the behaviour and characteristics of this battery are unfamiliar. Thus, the thesis purpose is to study and understand the state-of-art LTO battery cell behaviour under controlled situations.

LTO batteries require accurate battery models at different operating conditions due to its non-linear behaviour. Thus, extensive experimental characterization tests were developed to study the behaviour of the LTO battery to determine the dynamic behaviour of the LTO battery cell. The proposed model is suitable for various applications as well as for the development of Energy Management Systems (EMS) and Battery Management Systems (BMS). Hence, hybrid pulse power characterisation (HPPC) tests were developed and applied to a 2.9 Ah LTO battery cell. A second-order equivalent circuit (ECM) model is developed based on the experimental characterisation tests conducted at different SOC's (0 % - 100% at 10% interval) and operating temperatures (15°C, 25°C, 35°C and 45°C). The results of HPPC tests will be utilised for the parametrisation of the ECM. The ECM variables were incorporated into SOC estimation using the Coulomb counting (CC) method. The simulations model was developed in Simscape Matlab/Simulink software and were compared with experimental measurements for ECM validation.

KEYWORDS: Lithium titanate oxide (LTO), Equivalent circuit modelling (ECM), Hybrid pulse power characterization (HPPC) test, SOC estimation, Parameter estimation

Table of Contents

Figures

Tables

List of Abbreviations

Ah	Ampere hour
SoC	State of Charge
SoH	State of Health
OCV	Open circuit voltage
ESS	Energy storage systems
RES	Renewable energy sources
BMS	Battery Management System
EMS	Energy management system
NMC	Lithium Nickle Manganese Cobalt Oxide
NCA	Lithium Nickle Cobalt Aluminium Oxide
LTO	Lithium Titanate Oxide
ECM	Equivalent circuit model
SOEC	Second Order Equivalent Circuit Model
ABS	Acrylonitrile Butadiene Styrene
BVOH	Butenediol vinyl alcohol co-polymer
CCCV	Constant current/constant voltage

1 Introduction

1.1 Background and Motivation

Global warming and climate change are the biggest threat to humanity. The ever-increasing use of fossil fuels as a source of energy has led to the rapid growth of greenhouse gases (GHG) and the depletion of natural resources. The excessive use of fossil fuels has caused irreversible impacts on nature. As stated in the IPCC report of global warming effects of 1.5 °C due to the growing concentration of greenhouse emissions. The energy sector is one of the highest contributors to greenhouse gas growth (Allen et al., 2019). Ecological mindfulness and strict regulations in emission have increased the need for electricity generation in an eco-friendly manner, increasing land-based grid system demand. Recent demands on environmental sustainability have resulted in bringing an upsurge in the interest of batteries on a larger scale. This drive has translated into a range of development and integration of the energy system ranging from smaller handheld devices to electric vehicles. It is essential to move to cleaner and more sustainable form of energy sources.

The energy storage system (ESS) has been seen as a prominent technology to create an ecologically friendly and sustainable society. The energy storage system will play a vital role to increase the use of renewable energy sources (RES) significantly (Guo & He, 2018; Ibrahim, Ilinca, & Perron, 2008; Ng, Moo, Chen, & Hsieh, 2009). The use of energy storage systems to facilitate renewable energy sources in the current scenario will reduce climate change. Energy storage systems have now become a part of our day-to-day lives, primarily due to the research and development in handheld devices like portable devices, power tools, and electric and hybrid vehicles (Olabi, 2017).

Various energy storage technologies are available, but batteries have substantial potential for grid applications. Lithium-ion batteries are best suited for land-based grid

applications due to various features such as the higher power capability, faster response, low self-discharge rate and long cycle lifetime. Lithium-ion batteries have the ability to appease complex and large-scale development applications to the power grid (Chen et al., 2020; Stroe, Daniel-Ioan, Knap, Swierczynski, Stroe, & Teodorescu, 2016).

Lithium-ion batteries possess specific challenges as these batteries are not entirely stable under certain conditions such as higher temperature, which causes the battery to suffer from detrimental chemical reactions. Lithium-ion battery cells can rupture due to overheating or uncoordinated overcharging, leading to thermal runaway in the battery (Zhao, R., 2018). Lithium titanate oxide battery is a type of rechargeable Lithium-ion battery known for its faster-charging capabilities and low thermal runaway. Thus, making the battery safe to use. Therefore, LTO battery cells are regarded as crucial for the future of ESS (ASIAN DEVELOPMENT BANK., 2018)

It is essential to design and develop a suitable battery management system to observe the battery parameters to guarantee the safe operation of Lithium-ion batteries. Computer-aided simulations play a vital role in developing a battery system. Various elements affect the battery's performance at the system level, such as battery design, electrode morphology, battery chemistry, etc. Computer-aided simulations will help to predict these factors. Thus, modelling with computer-aided simulations plays an influential role in understanding battery characteristics and behaviour (Ceder, Doyle, Arora, & Fuentes, 2002).

An accurate battery model is indispensable to study the dynamic behaviour of the battery for different applications. Taking an already constructed battery into consideration, it is difficult to estimate and understand the battery behaviour under certain conditions required for the application. Battery modelling supports addressing this issue by testing the battery under certain conditions. The results of battery modelling help the user understand the battery’s dynamics at different conditions (Spotnitz Robert, 2005).

1.2 Thesis goals

The goal of this thesis is to analyse the dynamic behaviour of Lithium-ion battery under various parameters such as ambient temperature, state of charge, ageing, etc. Cell characterisation tests are conducted under these parameters in the laboratory. A comprehensive examination will be conducted on the battery to observe and understand the impact of temperature and cycling on the Lithium-ion battery during charging and discharging of the battery. The cell characterisation test will be prudently inspected to understand the battery performance and dynamic behaviour under different conditions. The conducted cell characterisation experiments on the battery will be utilised to develop an equivalent circuit model (ECM) to replicate its dynamic behaviour at operating conditions. Furthermore, the thesis also aims to provide a detailed procedure of computational simulations.

1.3 Research objectives

The cell characterisation tests will be carried out with Neware battery cell testing equipment (BTSDA-8000 model) and WEISS Technik temperature test chamber to regulate tests at different operating temperatures. The chamber will include a temperature sensor to monitor the internal temperature, as well as will employ temperature sensor probes to monitor the battery temperature during the experiments. The results acquired from these tests will be used to develop an ECM model for the Lithium-ion battery to understand the battery behaviour to predict and possibly extend the battery lifetime.

The LTO battery cell used in this dissertation is a pouch cell battery type. Pouch cell is known for higher packing efficiency. These pouch cells are known for the lower weight due to the exclusion of metallic materials for the outer extrusion and provide lower internal resistance as compared to lithium-ion batteries. Pouch cell is known for providing higher packing efficiency up to 90-90% (Linden, 1995).

Objectives of the study are as follows:

- Investigate the performance of Lithium-ion battery and different State-of-Charge (SOC) and observe the effects on capacity and internal resistance of the battery.
- Understand the impact of temperature and cycling on battery performance.
- Investigate the effect on capacity concerning temperature.
- Develop characterisation test procedures for Lithium-ion battery
- Conduct a hybrid pulse characterisation test on the battery chemistry.
- Parameterise ECM by utilising the least weight square methodology.

1.4 Structure of the thesis

This thesis shows the characterization and modelling of a Lithium titanate battery cell to understand the battery behaviour and performance in detail. The thesis is divided into six chapters and is described as follows:

Chapter 1 provides a brief description of the topic. The chapter also depicts the motivation behind this project. The chapter also describes the background study gap in this topic and briefly describes the research goals for the thesis.

Chapter 2 focus on a detailed explanation of the background study of the topic. The chapter describes the theoretical findings of Lithium-ion batteries evolution and the current scenario and compares different types of Lithium-ion batteries. Various types of battery modelling techniques are described in the chapter.

Chapter 3 describes the basics of characterisation tests and gives a brief understanding of the experimental equipment and procedure. The chapter also describes the developed battery cell holder in detail.

Chapter 4 provides a brief description of the battery modelling technique used in this thesis. It states the parameter estimation technique used and the SOC estimation

technique used in the equivalent circuit modelling. It describes the analytical observations from the simulations.

Chapter 5 summarizes the results of the experimental and simulated results. It shows a brief description of the comparison of the results

Chapter 6 summarizes the thesis and brings forward the main conclusion and future scope.

2 Lithium-ion Batteries - State of Art

2.1 Overview of Lithium-ion Battery

The first rechargeable battery was invented in 1859 by a French physicist Gaston Planté, based on lead-acid chemistry (Kurzweil, 2010). Since this invention, there has been considerable research and development in this field, especially in the last two decades based on battery chemistries, cell size, performance, etc. The traditional rechargeable batteries, which evolved around the late 1800's such as lead-acid and nickel-cadmium, faced various physical limitations primarily due to larger sizes and substantially heavy weight. These extensive designs also faced other constraints such as low specific energy, limited charging acceptance, high self-discharge rate (Scrosati, Garche, & Tillmetz, 2015). Lithium-ion batteries showed promising capabilities to overcome these conventional battery challenges. Lithium-ion batteries possess high specific energy and hold longer cycle life, making it easier to establish as one of the best battery chemistries available. Lithium-ion battery characteristics make it possible to have a broader base of application ranging from power components in handheld portable devices such as Mobile phone, Laptops, Tablets, etc., to the larger scale by playing a protagonist in energy sustainability (Zubi, Dufo-López, Carvalho, & Pasaoglu, 2018).

The need for higher density battery systems was realised and pursued since 1958 by analysing the solubility of non-aqueous electrolytes and Lithium. This study made it evident to pursue Lithium-ion batteries in commercial applications. Since the late 1960s, the market experienced an upsurge in demand for non-aqueous Lithium-ion primary batteries, which used Lithium sulphur di-oxide as the cathode (Harris, 1958). These batteries were predominantly used in military applications. These non-aqueous Lithium-ion batteries had certain safety aspects which needed to be elucidated. Thus simultaneously, improvements were observed in the understanding of intercalation of Lithium in different materials, starting the era of secondary rechargeable Lithium-ion batteries. In the last couple of decades, tremendous advancements have been seen in

Lithium-ion battery concerning physical and electrical capabilities (Reddy, Mauger, Julien, Paolella, & Zaghib, 2020). Today, Lithium-ion batteries size ranges from a coin with smaller capacities of around 5 mAh to more extensive and larger sizes with the range of 10,000 Ah.

The classification of electrical batteries is based on the capability of being electrically charged, viz primary (non-rechargeable) and secondary (rechargeable batteries. Lithium-ion batteries fall under the rechargeable battery family. In the early 1970s, due to the oil crisis, Stanley Whittingham, and other English chemists, started working on exploring the idea of rechargeable battery which can reduce charging time and lead to fossil-free energy in the future (Reddy et al., 2020). Exxon's experiments in the early 1970s did not yield success to Whittingham's team, and the project was halted.

John B. Goodenough further studied this project with a change in the battery's cathode element. In Japan, Akira Yoshino made another change in the anode by using carbonaceous material instead of reactive lithium metal. Thus, producing the first Lithium-ion battery prototype (Scrosati, 2011). Today, batteries have become so ubiquitous that it is almost invisible. In 2019, the Nobel Prize in Chemistry was awarded to John B. Goodenough, Stanley Whittingham and Akira Yoshino for their remarkable contributions to this development.

2.2 Working of Lithium-ion Battery

Lithium-ion batteries act as an electrochemical unit containing electrodes, separator and electrolyte. The rechargeable cell consists of three essential components, viz Cathode, Anode and Electrolyte (Manthiram, Muraliganth, Yamaki, & Tobishima, 2011). The storage mechanism is achieved by storing the energy in electrodes. The electrodes are made up of lithium intercalation compounds. The cathode is made up of substrate coated with an active material, whereas the anode is made up of thin copper substrate coated with active anode material. To avoid short circuit, a separator is placed between these two electrodes, preventing contact between these two electrodes (Warner, John,

2015b). The term anode designates to the electrode where during the discharge cycle, oxidation occurs. At the anode, oxygen is gained after the reaction occurs; the other electrode is a positive electrode known as a cathode. After the oxidation process occurs, electrons are released by the anode and are accepted by the cathode, causing a reduction reaction. These electrons require a material acting for the medium of transfer from cathode to anode and vice-versa. This gel-like liquid material operating as the catalyst is called the electrolyte. The roles of the electrodes, anode and cathode interchange depending on the direction of flow of current in the battery cell (Warner, John, 2015a).

The energy difference between the redox energies of the cathode and anode determines the cell voltage. This cell voltage depends majorly on the anode and cathode materials. Cell voltage can be co-related to Gibbs Free Energy (ΔG) and equilibrium cell voltage (E). Here, F represents the Faradays constant, and n stands for the number of moles. The occurrence of the reaction rate is determined by the electrolytic material (Manthiram, 2020).

$$\Delta G = -nFE \tag{1}$$

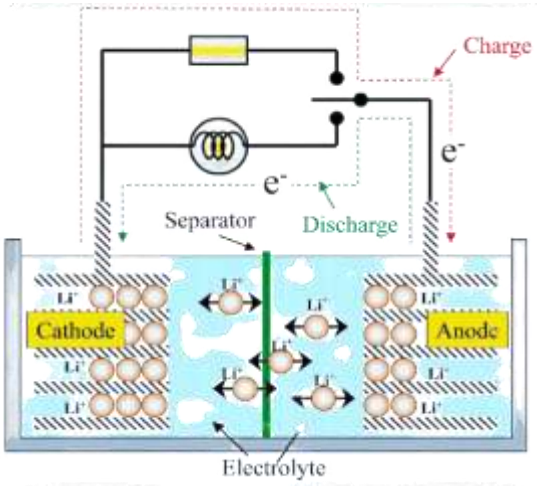

Figure 1 Working principle of a Lithium-ion battery – Schematic (Huang, Wang, Li, Ping, & Sun, 2015)

Figure 1 illustrates the working principle of the Lithium-ion battery. Figure 1 indicates cathode and anode electrodes with a separator in the battery's centre. These electrodes are submerged into an electrolyte, which carries positively charged lithium ions from the cathode to the anode and vice-versa through the separator. This movement creates free electrons at the anode. The separator blocks the flow of electrons internally between the electrodes of the battery. The battery composition or the chemistry is based on the materials used for cathode and anode. Some of the cathode materials used in Lithium-ion battery are oxides of lithium magnesium, lithium cobalt oxide, lithium nickel cobalt manganese oxide, etc. (Mishra et al., 2018). Similarly, the anodic materials change as per the battery chemistry, and some of these materials used for fabricating anode graphite carbon, hard carbon, lithium-titanate, tin-based alloys, etc. (Xu et al., 2014). The chemical reaction given below takes place in the $Li_xMn_2O_4$ battery during the discharge process:

At negative electrode:

$$LiyC_6 = C_6 + yLi + ye \quad (2)$$

At positive electrode:

$$Li_x - yMn_2O_4 + yLi + ye = Li_xMn_2O_4 \quad (3)$$

2.3 Lithium-ion battery chemistries

The state of art Li-ion battery cathode materials has been represented by lithium manganese oxide ($LiMn_2O_4$, LMO), lithium cobalt oxide ($LiCoO_2$, LCO), lithium iron phosphate ($LiFePO_4$, LFP) as well as cathodes containing mixtures such as the blend of aluminium in lithium nickel aluminium cobalt oxide ($LiNiCoAlO_2$, NCA) and lithium nickel manganese cobalt oxide ($LiNiMnCoO_2$, NMC) (Hannan, Hoque, Mohamed, & Ayob, 2017). In some cases, graphite is used for anode materials. In some instances, lithium titanate oxide ($Li_4Ti_5O_{12}$, LTO), tin or alloys are used (E. Chemali, M. Preindl, P. Malysz, & A. Emadi, 2016).

The demand for Lithium-ion batteries is continuously rising as the need for ESS is seen in various applications. The requirements for the Lithium-ion batteries varies as per the application. Lithium-ion batteries are used for grid applications, electric vehicles, handheld devices, etc. This range of applications constitutes various requirements from the battery. These batteries are now heading into aerospace and military applications on a larger scale. Compared to the traditional Nickel-cadmium and Lead-acid batteries, Lithium-ion possesses various advantages such as longer life, high energy density, high voltage capacity, etc. The major demerit of Li-ion battery is the cost of manufacturing (Stroe, Daniel Ioan, 2014).

Thus, various electrochemical storage systems, particularly Li-ion rechargeable batteries, have been developed over the period to focus on different market requirements (Warner, 2015). There are many different battery Li-ion chemistries based on their cathode and anode electrode material composition. Therefore, it is necessary to understand the basic cell chemistries of the Li-ion batteries to evaluate the merits and demerits for each application. Some of these Li-ion battery chemistries are described below:

2.3.1.1 Lithium Nickel Manganese Cobalt Oxide (NMC)

Lithium nickel manganese cobalt oxide is one of the most widely used battery chemistries. It is made up of a cathode combination of nickel, manganese and Cobalt. Hence, it is known as the NMC battery. NMC battery has been of great importance in the development of Li-ion batteries. It is regarded as one of the critical pillars of advanced Li-ion battery (Dong et al., 2019). The cathode of the NMC battery consists of around 10-20% of Cobalt.

In some cases, but generally consists of one-third of nickel, manganese and Cobalt each. NMC battery has been the most common use battery types. Thus, it is cheaper and a safe battery type as it has reduced risks of thermal runaway problems. NMC has a lower capacity but is known for its continuous discharge current. For e.g., In an optimised cell

NMC has a capacity of 2,000 mAh but can deliver continuous discharge of about 20 A current (Buchmann & Cadex, 2001). Figure 2 below describes the relative performance, safety and functional characteristics of NMC.

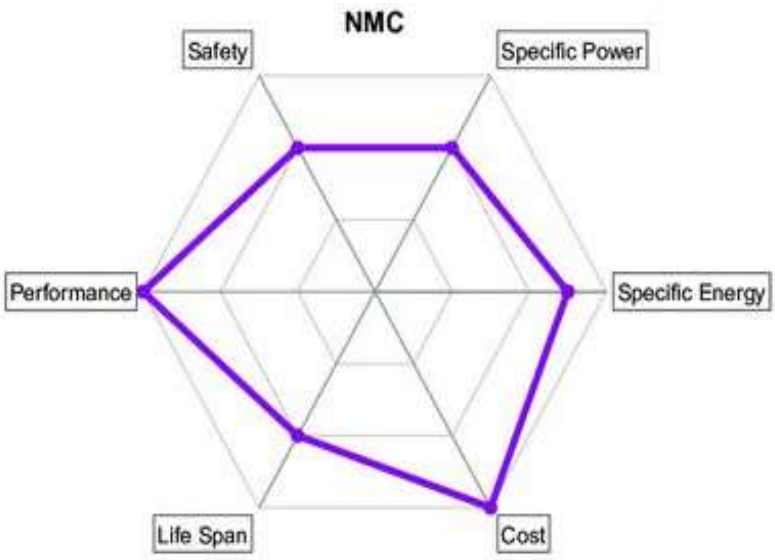

Figure 2 Lithium Nickel Manganese Cobalt Oxide Battery (NMC)

2.3.1.2 Lithium Nickel Cobalt Aluminium oxide (NCA)

Lithium Nickel Cobalt Aluminium Oxide battery is also known as NCA battery. It has been in the market since 1999 for various applications. Lithium Nickel Cobalt Aluminium Oxide is one of the batteries which has started to gain importance due to its use in powertrains and grid storage systems due to its increased energy density. In the case of batteries, geopolitical influence plays a vital role in the need for material. Today the cost of NCA battery is not the highest as compared to other battery chemistries, but the requirement of Cobalt, Lithium and Nickel increases the cost of the battery significantly as Cobalt is mainly produced in the Democratic Republic of Congo and the rising demand will increase the cost of this battery in future (Buchmann & Cadex, 2001). Figure 3 below illustrates the NCA battery's relative performance, safety, and functional characteristics.

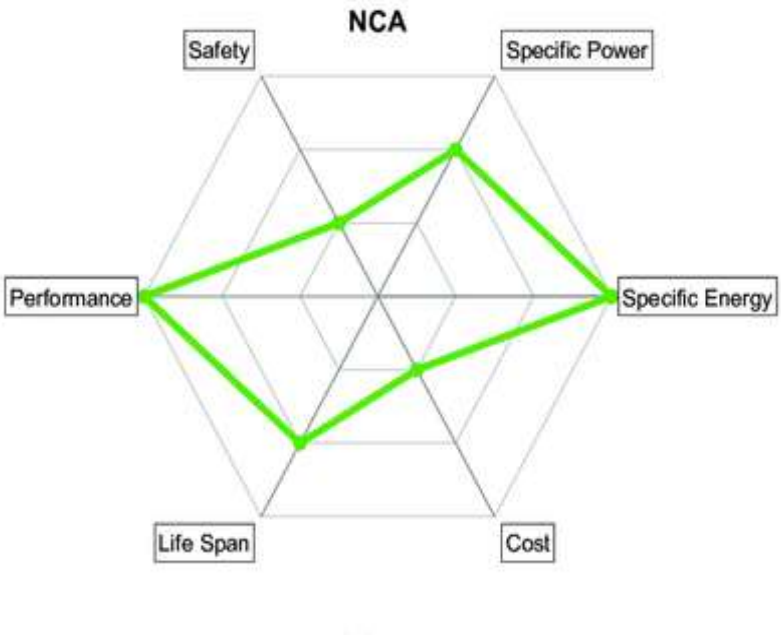

Figure 3 Lithium Nickel Cobalt Aluminium Oxide (NCA)

2.3.1.3 Lithium Titanate Oxide (LTO)

Lithium titanate oxide battery has been known since the 1890s but has seen significant interest over the last decade. Unlike the other types, this battery replaces the graphite material used for the anode electrode with an LI-titanate material known to form spinel structures. The cathode in this battery is similar to that of the NMC battery. This anode material creates "tunnel" like structures in three dimensions where lithium-ions are inserted. It is commercially one of the most successful anode materials due to its superior thermal stability, high life cycle and higher volumetric capacity (Nitta, Wu, Lee, & Yushin, 2015).

The use of lithium titanate nanoparticles at the anode instead of carbon helps in faster battery charging than other battery chemistries available. Lithium titanium oxide (LTO) provides approximately 175 mAh/g capacity but is thermally very stable. LTO is considered a "zero strain" battery because of its phase change, which is observed due to lithiation and de-lithiation, resulting in low changes in volume. The zero strain of LTO batteries helps in offering superior performances even at low temperatures, high power

and long cycle life. One of LTO batteries' other advantages is that no solid electrolyte interphase (SEI) layer is formed because of low operating voltages. Thus, there is almost no chemical reaction in LTO batteries due to lower operating voltages. Therefore, lithium titanate as an anode material shows excellent cyclic performances due to the voltage properties (Warner, John T., 2019b).

The table below illustrates the amount of series cell needed compared to lithium nickel manganese cobalt oxide battery. It can be observed to achieve 350V a system, only 95 NMC battery cells will be required to higher cell voltage, whereas approximately 160 LTO battery cells will be needed to achieve the same output.

	LTO	NMC
Cell voltage	2.2 V	3.7 V
Series cell needed to create 350V system	159	95

Table 1 Amount of series cell required to obtain same cell voltage

LTO batteries will play a vital role in bridging the gap between energy storage systems and grid power systems. As the urgency for the need for renewable energy increases, batteries need to be versatile in use, allowing synergy between battery storage, wind power and solar energy and the grid systems. LTO batteries could be used in achieving these goals due to their high-power capability horizon, making it suitable for land-based grid application. These applications require short bursts of high-power needs and high ramp rates. It possesses immense potential contributing to power system stabilisation (Nitta et al., 2015) (Madani, Schaltz, & Knudsen Kær, 2019).

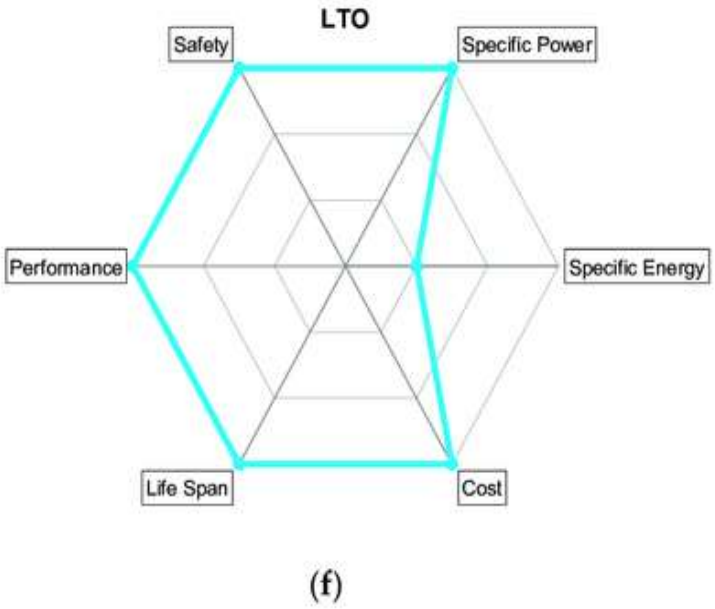

(f)

Figure 4 Lithium titanate oxide (LTO)

2.3.2 Comparison of battery characteristics

NMC can deliver either high specific energy or higher specific power but cannot offer both of these properties. Today it is used in Tesla Powerwall, LG CHEM RESU, etc. (Tesla powerwall.; LG chem RESU HV.). It is also used in some power tools as well as in powertrains. The low self-heating rate makes it one of the best candidates for electric vehicles. The main disadvantages of the NMC battery include its lower voltages than other systems and silicon added in graphite. It disforms the anode sizes while discharging and charging, resulting in mechanical instability in the cell (Buchmann & Cadex, 2001). The other challenge faced by NCM battery is structural degradation because of nickel rich combinations, reducing the overall battery cycle life. Cobalt rich combinations also suffer from safety concerns and higher costs (Warner, John T., 2019a).

The recent research and development in this battery have given it a prominent status in the market for high energy density applications. Lithium nickel cobalt aluminium oxide has a significantly higher capacity than Lithium nickel manganese cobalt oxide (NMC) and Lithium iron phosphate (LiFePO4). Thus, these batteries are used for moderate-rate applications with high energy density. NCA is highly regarded for its durability. NCA is also used in electronics devices and Panasonic, Sony and Samsung use NCA battery cells

(Buchmann & Cadex, 2001). NCA, unlike NMC, is not known for its safer purposes. It is one of the high-risk batteries that can work at the operating temperature of around -20 to 60°C at discharge and 0 to 45°C at charging (Eddahech, Briat, & Vinassa, 2015).

LTO battery cells are known for rapid battery charging and discharging. The abilities of the LTO battery, primarily due to higher stability, making it safer to use, no formation of SEI, greater performance at lower temperatures, longer cycle time, longer life, etc., makes it one of the best candidates for this thesis. Thus, LTO batteries have been seen in various applications, such as grid systems and e-mobility technologies. Therefore, it is regarded as one of the most prominent battery chemistries for the future and is considered for its potential for wind power system (Stroe, Ana-Irina, 2018). LTO batteries are acknowledged for their longer cycle life due to lower mechanical faults such as crack formation because of good cohesion between the electrodes, the current collectors and the separators. This ability of LTO battery cells makes it the best fit for applications with faster charging of batteries (Warner, 2019). One of the drawbacks of the LTO battery is reduced energy density as it can be used with low voltage levels around 1.5 -2.7 V. The low voltage operation also makes it challenging to operate at high voltage. Thus, the need for a higher number of battery packs at the system level is required (Buchmann & Cadex, 2001).

LTO battery structure is created of spinel's as compared to NMC and NCA, which consists of layered formation. NMC and NCA batteries are known for their high voltage levels ranging around 3.6 to 3.7 V, whereas LTO batteries have a lower voltage range of 2.4V (Burke & Miller, 2009). LTO batteries are considered one of the safest li-ion batteries available due to low thermal runaway (Adamec, Danko, Taraba, & Drgona, 2019). LTO batteries can be used for applications with lower operating temperatures as compared to NMC and NCA. LTO batteries have a longer cycle life of around 3000 to 7000 cycles, whereas NCA and NMC batteries have 500 and 1000 cycles, respectively. The table below illustrates a comparison of NMC, NCA and LTO battery cells (Buchmann & Cadex, 2001).

	NMC	NCA	LTO
Structure	layered	layered	spinel
Voltages	3.6 - 3.7V	3.6 V	2.4V
Capacity	150-220 Wh/Kg	200 -260 Wh/Kg	50 - 80 Wh/Kg
Charge (C- rate)	0.7 - 1C	0.7C	1C
Discharge (C -rate)	1C	1C	10C
Cycle Life	1000 - 2000	500	3000 - 7000
Thermal runaway	210℃	150℃	low
Operating temperatures	0 to 55 ℃	-10 to 60 ℃	-20 to 55 ℃
Safety	Medium	low	High
Applications	E-bikes, medical devices, etc	Medical devices, powertrains, etc.	UPS, electric powertrains, solar-powered street lighting, etc.

Table 2 Comparison of characteristics of NMC, NCA and LTO batteries (Adamec et al., 2019)

2.4 State of Charge (SOC)

The state of charge of the battery is defined as the current cell capacity; it is relative to its rated capacity in certain conditions but generally relative to its present capacity to reduce the error ambiguity. In other words, it is the ratio of current capacity (Q(t)) to the

nominal capacity (Qn). The nominal capacity is the capacity of a new cell and is generally provided by the manufacturer. The SOC level ranges from 0% to 100%, depending on the level of battery charge. In the case of grid application, it is defined in energy kilowatt-hours (kWh) (Abdi, Mohammadi-ivatloo, Javadi, Khodaei, & Dehnavi, 2017).

The battery's total capacity or nominal capacity is the maximum amount that can be drawn from a fully charged battery cell. This value varies as the battery life decreases due to certain factors such as temperature, ageing, etc. The residual capacity of the battery is the amount of charge that can be withdrawn from the current state of the battery compared to its nominal state (Narayan, 2017). Mathematically SOC is described as follows (Sundén, 2019):

$$SOC\ (t) = \frac{Q(t)}{Q_n} \tag{4}$$

SOC plays as a critical component in battery management systems as it describes the level of battery charge available, this also helps to evaluate various elements such as battery lifetime, development of BMS, battery ageing, EMS, etc. (Barré et al., 2013; Garcia, Fernandez, Garcia, & Jurado, 2009; Haq et al., 2014; Wikner & Thiringer, 2018). Various methods can be used to determine the SOC of a battery. These methods help estimate the SOC levels of the battery. It is vital to have higher accuracy, smoothness, and high robust SOC estimation techniques to achieve high efficiency and safety. Figure 5 below illustrates the various definitions of SOC of a battery (Baba & Adachi, 2014).

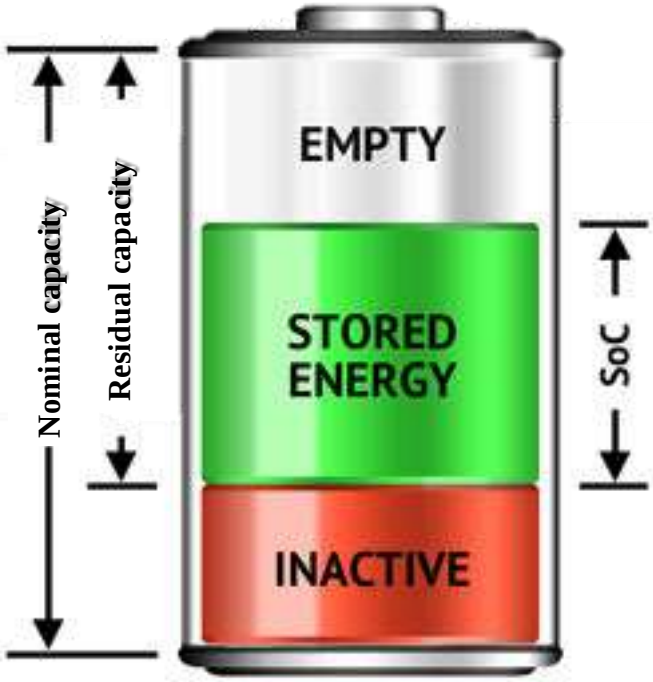

Figure 5 SOC definitions of a battery

The SOC of the battery can be estimated through various method possible; the primary classification is of these methods is given below as follows:

- Direct measurement – This method is known to be dependent on the physical properties of the battery. This method works mainly with the voltage and impedance of the battery cell. In some of its methods, longer rest times are required increasing the time consumption for this system. It has lower dynamics and is sensitive to temperatures.
- Book-keeping estimation – The book-keeping method uses the discharging current as of the input and integrates it over time to calculate the SOC. It is suitable for tracking rapid changes in SOC levels.
- Adaptive systems – Adaptive systems are delf design system which can adapt and adjust the SOC for various discharging conditions. It is regarded as the future for SOC estimation, but it requires heavy training data for higher accuracy.
- Hybrid methods – A global optimal estimation performance is available from this method as it benefits from various advantages of the SOC estimation. They are

known to show the highest accuracy as compared to the rest but require heavy data as well as being time-consuming (Chang, 2013) (Ng et al., 2009)

2.5 Open circuit Voltage (OCV)

Open circuit voltage (OCV) is defined as the potential difference between the positive and negative electrodes of the battery cell when there is no current flow and the cell is in an equilibrium state. In other words, it can be described as the steady-state voltage at a terminal of a battery under open circuit condition. OCV also plays an important in understanding the performance of the battery. OCV is modelled as an ideal voltage source. The OCV of a battery is highly affected by a change in SOC of the battery; similarly, temperature also affects the OCV. The OCV-SOC relation differs from battery chemistries as well as per different temperatures and ageing of the battery. Thus, OCV-SOC relation has been studied in this thesis by conducting tests at different SOC levels and temperatures for both charging and discharging (Chang, 2013).

2.6 Battery modelling techniques

The non-linear performance of Li-ion batteries makes modelling the dynamic behaviour extremely difficult. This non-linear nature is also affected by various other parameters such as SOC, operating temperature, ageing, current rate, etc. Li-ion batteries are generally modelled as an ideal DC voltage source or mathematical models (Aristizábal et al., 2019; Tariq, Maswood, Gajanayake, & Gupta, 2018). Math based kinetic battery models (KBM) were initially developed for lead-acid batteries. Although KBM were widely popular, they failed to investigate the non-linear behaviour of the battery. Later, researchers developed a wide range of models depending on the complexity to model the batteries (Chauhan, Reddy, Bhandari, & Panda, 2018; Manwell & McGowan, 1993; Thanagasundram, Arunachala, Makinejad, Teutsch, & Jossen, 2012a).

There are various battery modelling methods such as electrochemical, electrical equivalent circuit modelling, thermal models, empirical models, etc. These battery

models have different approaches depending on the level of complexity, accuracy and parameterisation requirement depending on the application of the battery. Battery modelling has been classified into four main sections: Empirical models, Equivalent circuit models, electrochemical models, and data-driven models. These models are derived from electrochemical modelling and thus, play a different role in modelling a battery. Some of these models are described in this section (Meng et al., 2018a). Figure 6 below illustrates the classification of battery modelling:

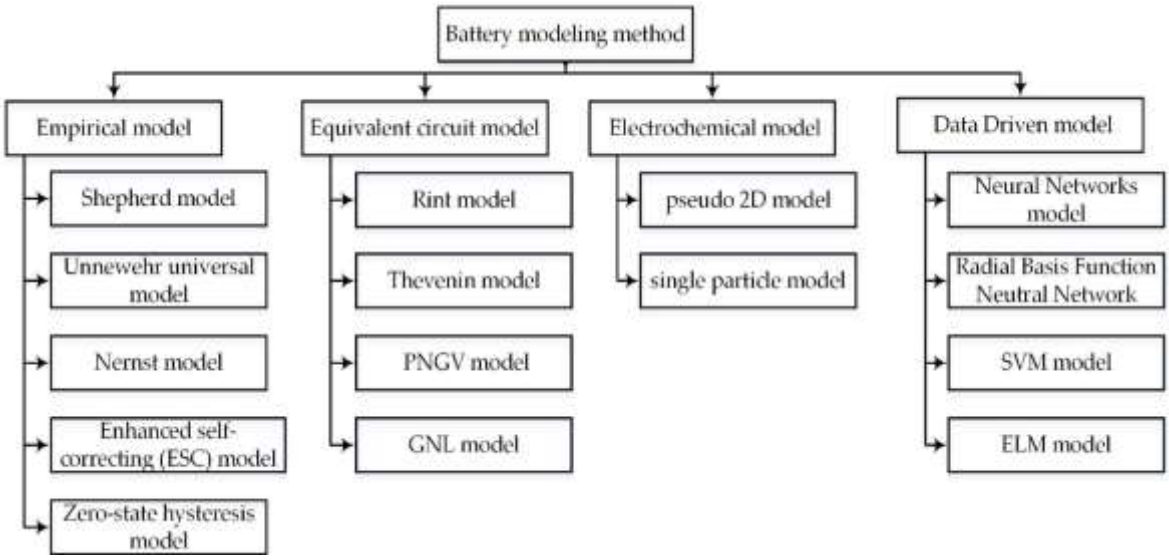

Figure 6 Battery modelling method - classification (Meng et al., 2018b)

2.6.1 Electrochemical Model

Electrochemical models, as the name suggests, work with the electrochemical process inside the battery during the battery charging and discharging, which provides the user precise information about the lithium concentrations and the over-potentials in the battery. This information is vital to reduce specific side effects in the battery to keep the battery in safer conditions. This model was developed by Doyle-Fuller-Newman, depicting important aspects in Lithium-ion battery such as reaction kinetics, diffusion and migration (Doyle & Newman, 1995). The Electrochemical models are further classified into two types, viz: pseudo 2D model and single-particle models. The

electrochemical models are known for its computational efficiency providing higher efficiency in voltage calculation. The main disadvantage of using this model is the complexity involved due to the use of partial differential equations, which can increase decrease the accuracy in different conditions (Tomasov, Kajanova, Bracinik, & Motyka, 2019) (Dees, Battaglia, & Bélanger, 2002)

2.6.2 Empirical Model

In this type of battery modelling, the terminal voltage is described as the voltage used for representing the SOC and current mathematically. This type of modelling is considered the simplified version of electrochemical battery modelling. The polynomial expression in this model is reduced compared to the electrochemical model as it represents the required non-linear characteristics of the battery. There are five categories in the empirical model, and they are as follows: Shepherd model, Unnewehr universal model, Nerst model, enhanced self-correcting model and zero- hysteresis model. The empirical models are known for its simplicity, but this affects the model's accuracy as it limits the capability of describing the terminal voltages (Moore & Eshani, 1996). Further comparison between empirical models and equivalent circuit models is described by Hussein (Hussein & Batarseh, 2011)

2.6.3 Data-driven model

This method uses different data mining methods, which are rapidly developing in the current scenario. The use of machine learning is the base of data-driven models used to draw relations between various variable required for estimation without any prior knowledge. This type of battery modelling requires sample data that acts as the historical data of the measurement, which is established from the training process. This model uses the historical data and compares it with real-time data to estimate the behaviour intended depending on different scenarios considering the required parameters: SOC, temperature, voltage and current. There are four types of data-driven models: neural network, SVM model, radial basis function neural network model and ELM models

(Meng et al., 2018c). This model type is known for its accuracy as well as no prior knowledge is required for running this model. The disadvantage of using a data-driven model is difficulty in collecting training data samples which can significantly affect the accuracy of the model (Li, He, Su, & Zhao, 2020; Meng et al., 2018).

2.6.4 Equivalent circuit model

Electrical equivalent circuit models (ECM) use a combination of electrical components by lumping together battery dynamic such as voltage, resistors, capacitors as well as certain non-linear elements. The ECM consist of an open circuit voltage source with specific electrical parameters. It uses resistor-capacitor branches and current inputs. It is one of the most widely used battery modelling techniques due to its high accuracy and sufficient complexity. The design of ECM models is simple and depends on the user's accuracy requirement, which also reduces the computational simulation requirement significantly. ECM models are made up of three major parts, viz; static part to represent the thermodynamics of the battery chemistry, a source and load and a dynamic part determining the cell impedance behaviour (Yann Liaw, Nagasubramanian, Jungst, & Doughty, 2004). ECMs are less complex as compared to empirical models. ECM models are known for the representation of static and dynamic behaviour. Thus, ECM is considered the best option for operation with the use of Kalman filters and least square-based filters. Therefore, ECM models are best implemented for the benefit of BMS systems. The ECM is categorised into four types, namely the RINT model, Thevenin models, PNGV model and GNL model. (Waag, Fleischer, & Sauer, 2014)

The ECM model subcategories are interrelated concerning the model's design and are used depending upon the accuracy and complexity requirement. Thevenin's model is generally preferred in many applications due to sufficient accuracy and complexity. Thevenin's model considers all the significant electrical parameter, and it has higher accuracy than the RINT model. In its most basic forms, Thevenin's model consists of an open circuit voltage source followed by a series resistor and an RC parallel branch, used to estimate the transient load voltages at different SOC levels (Bustos, Siddique, Cheema,

Gadsden, & Mahmud, 2018). Figure 7 below illustrates Thevenin's' model representation:

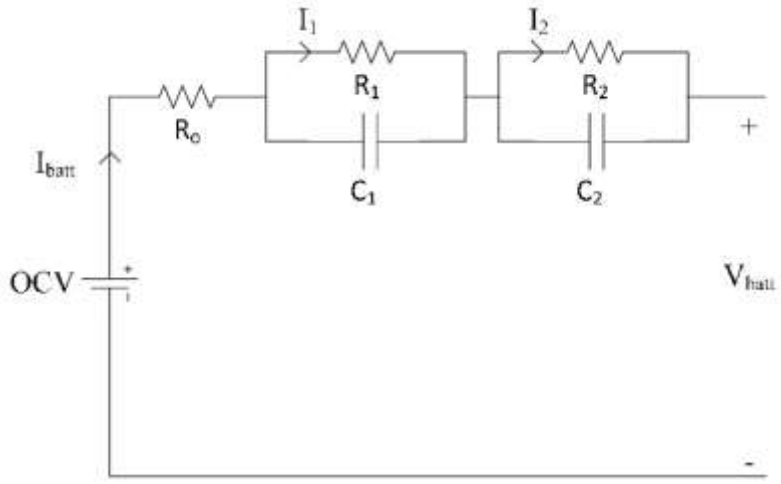

Figure 7 *Thevenin's second-order equivalent circuit*

The second-order equivalent circuit model is one of the most popular models due to the simplicity and high accuracy rate. Figure 7 above describes Thevenin's second-order circuit; it consists of an open circuit voltage source followed by a series resistor. It is further series connected to two parallel RC branches. These RC branches consist of activation polarisation represented by R1 and R2 and similar concentration polarisation byR2 and C2 in the second branch. Thevenin's model is extensively used, but after the second-order, the accuracy change is negligible but increases the computational time and complexity. Thevenin's second-order equivalent model is regarded as the benchmark in lithium-ion battery models. Thus, this dissertation uses a second-order equivalent circuit for battery performance modelling of the LTO battery cell (Arunachala, 2018).

3 Characterisation analysis of LTO battery.

Lithium-ion batteries are used widely in the field of smart grid application for various purposes. The need for these applications changes from time to time as different goals are to be achieved. The performance of any battery is needed to be assessed before it is employed for any application. Similarly, the battery behaviour and lifetime are required to be monitored and necessary steps need to be taken to enhance these parameters. This is achieved by using a Battery management system (BMS). Several parameters affect the battery behaviour and performance, such as the State of Charge (SOC), temperature, open-circuit voltage (OCV), cell polarisation, etc. (Hua, Zhang, & Offer, 2021).

Lithium titanate batteries are increasingly used in various applications, particularly in the field of grid application. It is necessary to evaluate the performance and behaviour under various circumstances. It is essential to predict the batteries behaviour and performance under different operating conditions such as temperature and SOC levels. Battery modelling is a set of equations used under a particular condition, depending upon the requirement, complexity and accuracy and is significant in predicting the behaviour of the battery (Wang, Jiang, Li, & Yan, 2016). There are various performance models available which consider multiple aspects of the battery to assess the required strategies and requirement of the battery for a certain ESS. Although modelling of a battery is a complex methodology due to the non-linear behaviour, it is essential to use an accurate modelling type for any battery as per the need of the application. Therefore, in this thesis, the performance modelling of the LTO battery cell is performed by using a second-order equivalent circuit; the parameter estimation required for the modelling for the battery is achieved by conduction extensive laboratory tests, as explained in the following section.

3.1 Characterization LTO battery cell

LTO battery is being used in various applications such as grid systems which makes it very important to understand the behaviour of the battery under different conditions. Li-ion batteries are non-linear systems that are complex due to electrochemical processes, various dynamic parameters, internal resistance, capacity, open-circuit voltages, etc. Thus, it becomes imperative to model the performance of the battery. As stated in the previous section, various models require different parameters to provide useful information to estimate the battery behaviour. It is crucial to parameterise these functional elements required for modelling with maximum accuracy. In order to thoroughly parameterise the battery performance modelling, comprehensive laboratory tests are needed to be performed (Stroe, 2018).

Thus, a procedure has been developed to characterise the battery behaviour under monitored conditions: at four different temperature levels (15°C, 25°C, 35°C and 45°C) inside a thermal chamber as well as at different SOC level – at 10% interval ranging from 100% - 10 %. This characterisation test is called as Hybrid Pulse Power Characterization (HPPC) test. The HPPC tests are widely popular and recommended by the U.S. Department of Energy as it is used to determine the internal resistance, capacity, open-circuit voltage under the required conditions (Belt, 2010). Details of this methodology are presented in the further sections.

3.2 Lithium-ion battery cells used in this research

The table below describes the LTO battery cell specifications used in this project:

Product Name	LTO Battery Cell
Rated capacity	2.9 Ah
Nominal Voltage	2.4 V
Minimum Voltage	1.6 V
Maximum Voltage	2.6 V

Table 3 LTO battery cell specifications

3.3 Battery cell holder

The LTO battery used in this thesis is a pouch cell and the battery dimensions are 10 cm in height, 6 cm in length and 1 cm in width. The LTO battery, with the weight of the higher cross-sectional cables attached to the battery and with lower battery width, makes it difficult for the battery to be in the upright position. Thus, it was necessary to develop a battery holder for the battery cell. The battery holder was designed using Autodesk Inventor software.

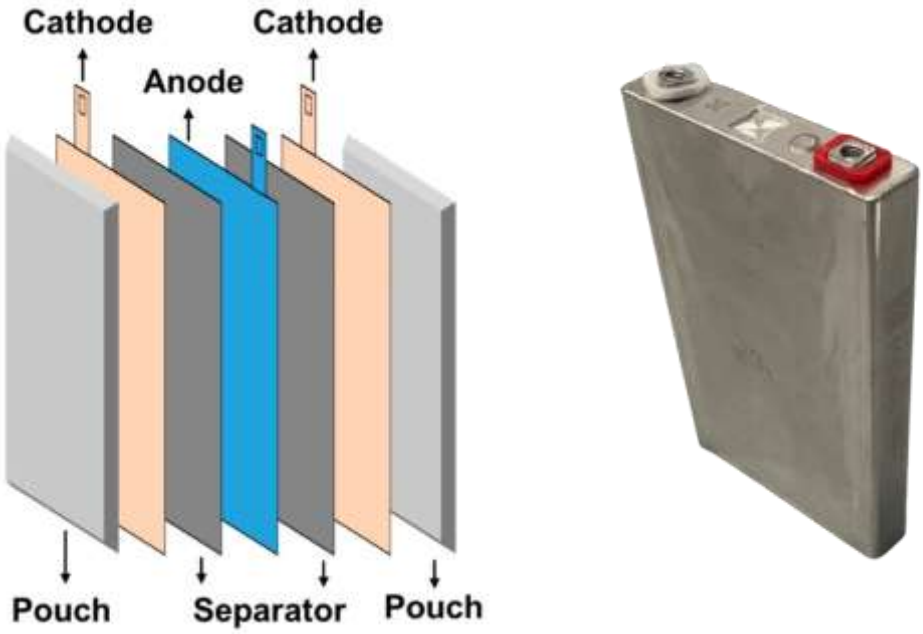

Figure 8 Construction of pouch cell and 2.9Ah LTO battery cell (from left to right)

The battery cell holder was developed using the Autodesk Inventor software. The design of the cell holder is simplistic in nature; it works as the battery cell holder with the battery being placed on the top. The battery holder is rectangular in shape, similar to the battery and has sufficient room for air to travel to avoid battery heating due to the holder. The battery holder is 10 cm in height, 10 cm in length and 3.6 cm in width. The battery holder contains a cavity for the battery to be placed with is 7 cm in height, 7 cm in length and 1.6 cm in width. The cavity is provided with extra space in length and width to allow enough room for the battery during the expansion due to higher operating

temperature. The battery holder cavity is enough to place around 70% of the battery height so that sufficient room is provided for the cable to be connected, blocking any contact between the 3D printing material and open cables.

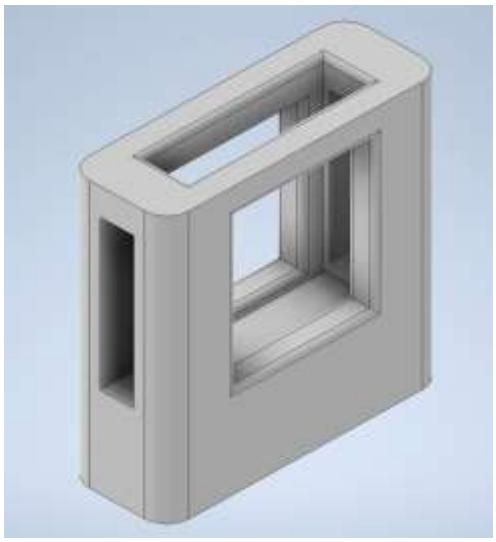

Figure 9 3D printed battery holder design (Autodesk Inventor)

The battery cell holder was manufactured with the Ultimaker S3- 3D printer. The Ultimaker 3D printer utilises various types of filaments for 3D printing, such as ABS, PLA, PTEG, etc. As the experimental tests were conducted at temperatures above 40 °C, the material used for the 3D printed holder used was Acrylonitrile Butadiene Styrene (ABS). ABS is an opaque thermoplastic and amorphous polymer. This polymer is very popular due to its temperature withstanding heat and resistance to impact. The material can withstand temperatures ranging from -20°C to 80°C, making it the best candidate for the project (Wojtyła, Klama, & Baran, 2017). Ultrafuse Butenediol vinyl alcohol co-polymer (BVOH) water-soluble support filament was used for the 3D printing. Figure 9 above illustrates the design of the battery holder. The structural opening in the design helps in reducing unnecessary temperature rise to allows airflow throughout the structure. The design consisted of 30% infill with grid mesh infill patterns reducing the weight and maintaining the overall strength.

Figure 10 3D printed battery cell holder

3.4 HPPC characterisation test

The HPPC test procedure consists of high current charge/discharge pulses; the effects of these pulses are utilized to calculate the battery cell's pulse power and various energy capabilities. The HPPC test is generally employed while using ECM modelling technique and multiple studies are conducted using simple resistor and resistor-capacitor branches for ECM models. The parameters obtained from the HPPC test are used in modelling the ECM mode as well, as it helps to comprehend the relationship between various elements such as OCV – SOC. The primary purpose of the HPPC test is to measure resistance and power during charging and discharging at different SOC levels (Pattipati, Sankavaram, & Pattipati, 2011; Samadani, Lo, Fowler, Fraser, & Gimenez, 2013; Yuan, Wu, & Yin, 2013).

The HPPC test procedure consists of various steps required to measure the dynamic power capability of the battery during both the charging and discharging pulse of the battery. The HPPC test approach is used to linearise the battery behaviour at a certain point of life centred on repetitive test cycling nature at different SOC levels of the battery and different temperature conditions. This test is intended to result in understanding the battery behaviour under these conditions. As LTO battery is known for its working at lower as well as higher temperatures as stated in the earlier section, the HPPC test aims

to examine the battery behaviour at 15°C, 25°C, 35°C and 45°C (Zhang, Mu, Zhang, & Han, 2014) (Buchmann & Cadex, 2001).

HPPC test is utilised to estimate the parameters required for the second-order equivalent circuit. The HPPC test can precisely describe the internal characterises of the battery, which is vital due to the relationship between operating conditions and model parameters. In the HPPC test measurement, current pulses are applied during the discharging of the battery for few seconds. Thus, different parameters can be identified by studying the corresponding part of the battery voltage response. The battery cell impedance is known to be affected by parameters such as SOC, temperature, current, etc. Therefore, it is recommended to conduct an HPPC test at different temperatures and SOC levels (Yang, Xu, Cao, & Li, 2017) (Stroe, Ana-Irina et al., 2018) (Arunachala, 2018). The following section describes certain important technical aspects required for studying the HPPC test procedure.

3.5 Experimental set-up

The experiment of the HPPC test is conducted under a controlled environment on the LTO battery cell to control the temperature during the experiment. Thus, the use of the WEISS Technik climate test chamber was employed. This temperature chamber is used to control the temperature at four different temperatures. The experiment requires Neware Battery Cell Testing Equipment (BTS8000 model). The Neware equipment enables to record data at an application frequency of 10 Hz. The following section illustrates the experimental setup used in the thesis.

High power 2.9 Ah LTO battery cell was used in the HPPC experiment. The specifications below indicate the model specification for Neware BTS-8000 equipment used in the thesis:

Channels per unit	4
Four wire measurement	Yes
Maximum charging current (A)	300
Minimum charging current (A)	-300
Voltage range during charging/ discharging (V)	+5 to 0
Time resolution (ms)	1
Current range (Charge/Discharge)	1A to 300A

Table 4 Neware BTS-800 model specification

Figure 11 below illustrates the WEISS Technik weather chamber and Neware Battery Cell Testing Equipment (BTSDA 8000 software model) used in the experiment:

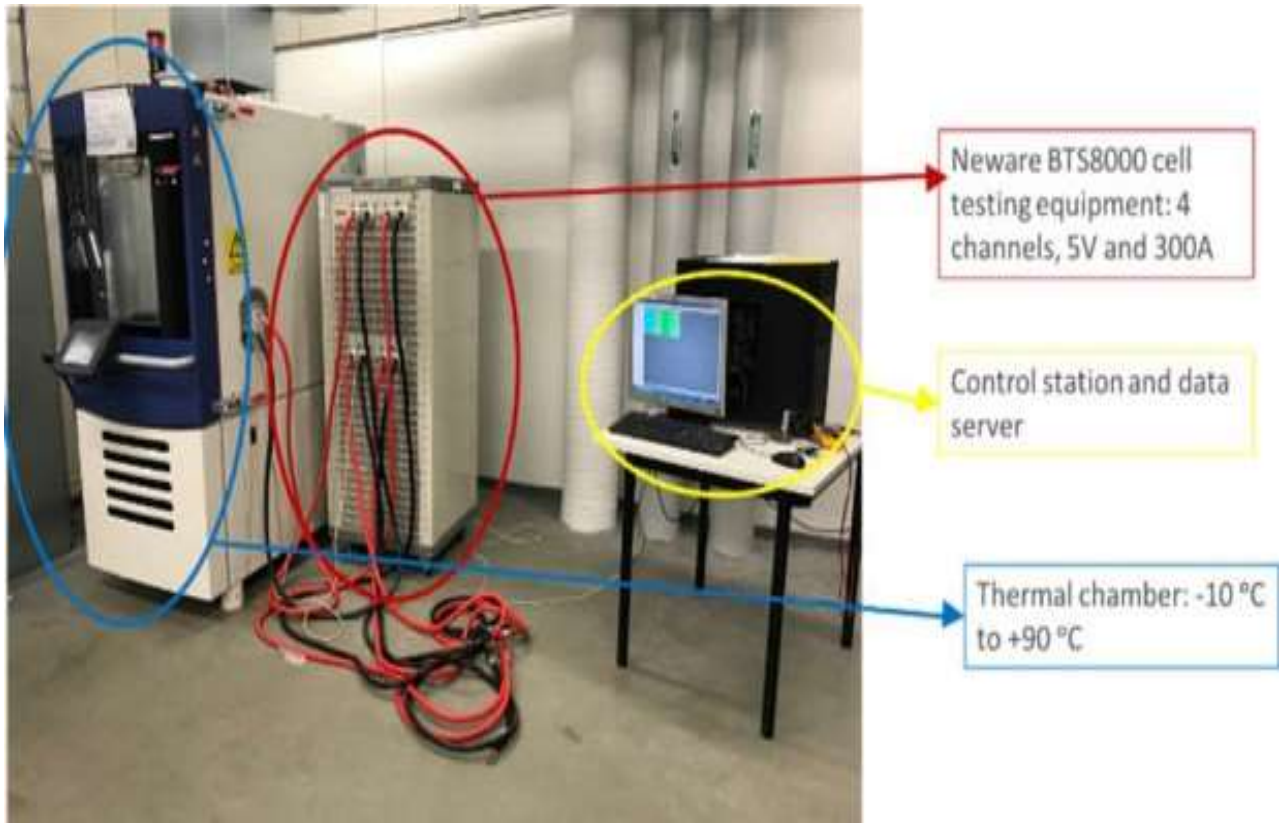

Figure 11 WEISS Technik weather chamber and Neware BTS-8000 model

The battery is connected with a thermocouple which helps to monitor the battery temperature due to the difference between battery temperature and internal temperature due to battery characteristics. The battery cell is connected to the battery testing equipment with AIV 20 mm^2 cross-section power cables with ring terminals. Figure 12 below indicates the LTO battery connection with the Neware battery cell testing equipment:

Figure 12 Experimental set-up of LTO battery in WEISS Technik Weather chamber

The basic HPPC test is generally started directly by charging the battery, but in this project, for safety reasons and higher stability, the charging and discharging was first implemented, followed by the HPPC test. The battery charging and discharging test involves connecting the battery and resting the battery in the thermal chamber for 1 hour. The battery is then charged with a constant current/constant voltage (CCCV) charge pulse until the upper cut-off voltage limit is met. The upper voltage cut off for the Toshiba battery is 2.9 V. A rest of 10 minutes is provided for the battery to settle at the cut off voltage. A constant current discharge pulse follows it up to the rated voltage

requirement: this is followed by a rest of 10 minutes. Thus, the charging and discharging of the battery is completed. Figure 13 below illustrates the constant current charging and discharging curves representing current on the y-axis and time on the x-axis.

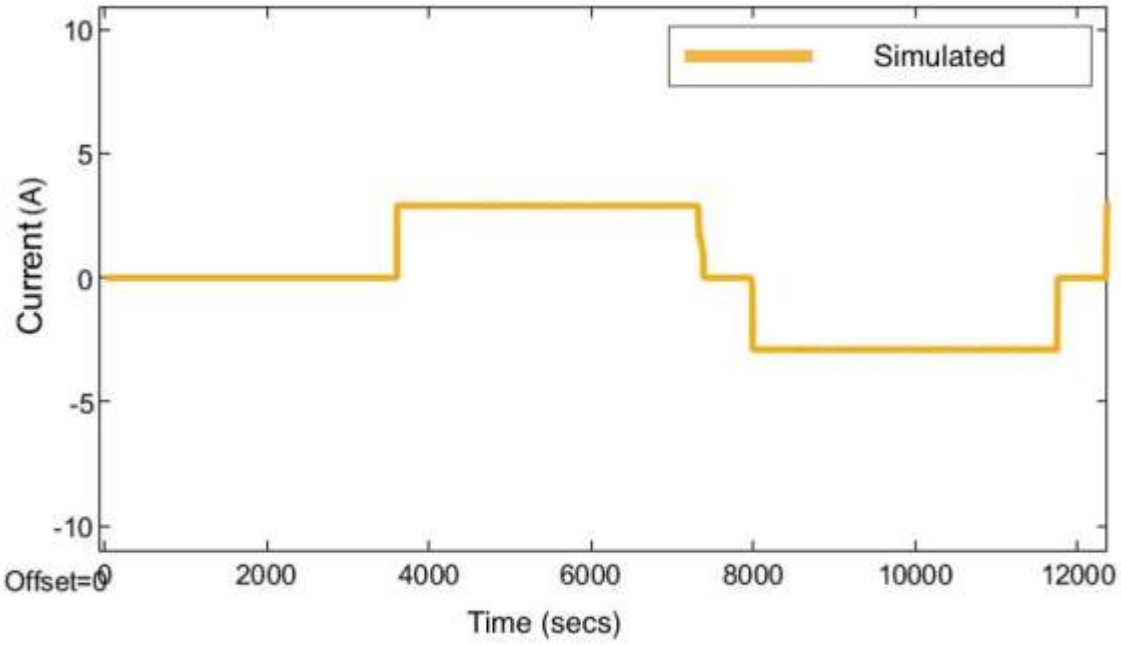

Figure 13 Schematic representation of the constant current curve

The procedure for the HPPC test is conducted after the charging-discharging is completed. In this test, the cells were pulse discharged at 10% SOC step starting from 100% SOC, i.e., fully charged battery. The procedure for the HPPC test employed in this thesis is described as follows:

1. Fully charging the battery to the upper cut of voltage with CCCV pulse (2.6 V)
2. Resting the battery for 1 hour to obtain the equilibrium
3. Applying a Constant Current (CC) discharge pulse for a span of 10 s
4. Resting the battery for 40 s
5. Applying a Constant Current (CC) charge pulse for 10 s
6. Discharging the battery until the next SOC step is reached

The procedure repeats steps 3 – 6 until all SOC levels are reached and for different temperatures. Figure 14 below shows the HPPC test results - current profile. The results for other temperatures are discussed in the results and discussion chapter.

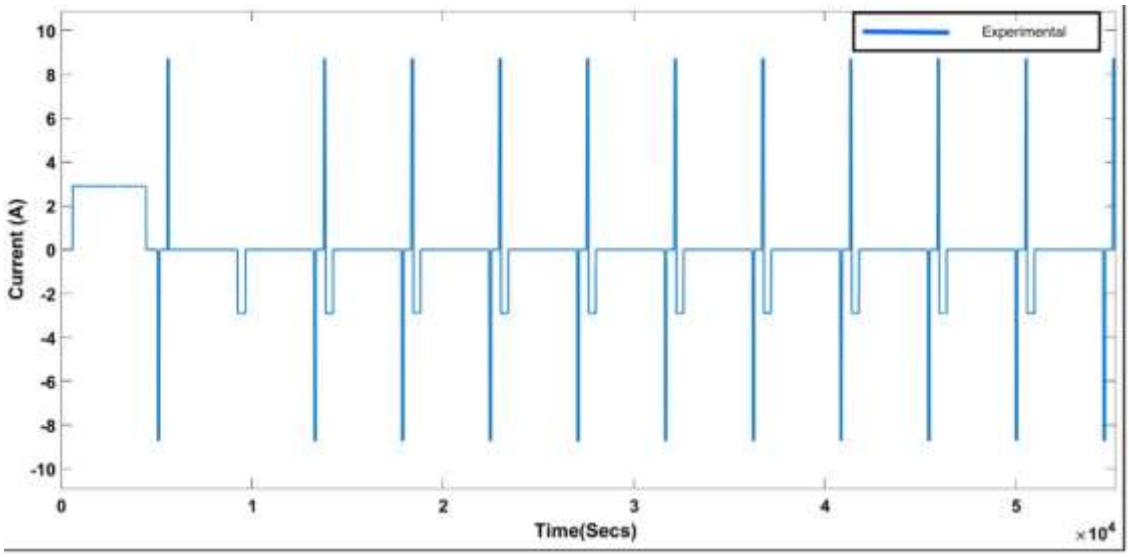

Figure 14 Current profile from HPPC test

4 Modelling of LTO battery cell

As described in section 2.6.4, Thevenin's second-order equivalent circuit model is the most suitable modelling technique for this thesis. Thevenin's second-order equivalent circuit is known for its versatility and will successfully emulate the parameters required for the modelling methods. Given the necessary experimental analysis, this technique will emulate the working of Li-ion batteries at different operating conditions, i.e., SOC, C-rate, temperature and ageing. This modelling technique replicates the hysteresis effects in the cell and its self-charge characteristics, too (Parthasarathy, Hafezi, & Laaksonen, 2020). The ECM technique is stated as a stated benchmark model for Lithium-ion batteries due to its accurate depiction of diffusion, charge transfer and solid electrolyte interface (SEI) reaction in the form of the resistors and capacitors (Gao, Zhang, Yang, & Guo, 2018).

The proposed Thevenin's second-order equivalent circuit (SOEC) is illustrated in Figure 15 below. This proposed model uses variable parameter reading documented during the HPPC tests performed at different temperatures and SOC levels. The circuit parameters required in the ECM modelling technique are determined from the HPPC tests conducted in the laboratory. These recorded parameters from the experimental tests are used to parametrise the required ECM elements, which is stated in the following section. The proposed SOEC cell model is developed using the Simscape platform of Matlab/Simulink.

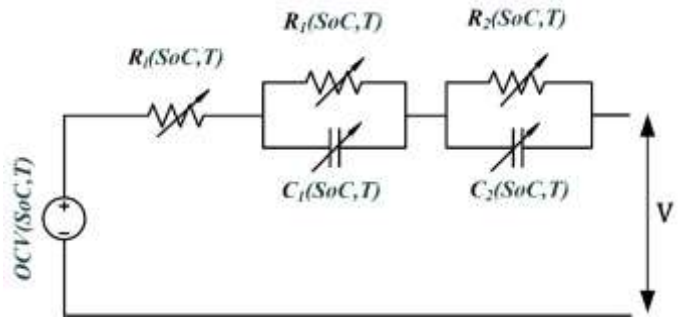

Figure 15 Proposed second-order equivalent circuit

4.1 Parameter Estimation

The OCV is recognised as the protagonist for the parameter estimation and identification of the battery system as it is strongly related to the State of Charge (SOC) of the battery and State of Health (SOH). The relationship between the OCV and SOC curve is very useful in understanding the battery characteristics such as SOC estimation and SOH estimation. This is vital, especially when using a Battery management system (BMS) for simulating the internal battery charge and discharge with the highest accuracy. Thus, a physical model is preferred for applications such as grid systems which require higher efficiency and accuracy. Thevenin's second-order equivalent circuit is best suited for this purpose (Locorotondo, Berzi, Platz, Nuffer, & Rauschenbach, 2018).

The SOEC is known for its accuracy and flexibility and can be embedded into a micro-controller to provide real-time results of the battery output. The components in this SOEC include the open-circuit voltage and the series resistance (Ri) followed by the two parallel polarisation networks viz: R1, C1 and R2, C2. The OCV, as stated earlier, is an essential component in this system; it states the ideal voltage generator and is variable concerning the SOC. The series resistance Ri) represents the internal resistance in the system responsible for the voltage drop and rise during the charging and discharging process. The first parallel polarisation network with components R1 and C1 is known for representing the faster dynamics that depict the battery surface effects on the electrodes and the reaction kinetic. These components individually represent the charge transfer resistance (R1) and double-layered electrochemical capacitance (C1). The second polarisation network with components R2 and C2 are representing the slower dynamics of the battery system. The diffusion process and the active network in the battery are more dependent on this network (Lee et al., 2006; Thanagasundram, Arunachala, Makinejad, Teutsch, & Jossen, 2012b).

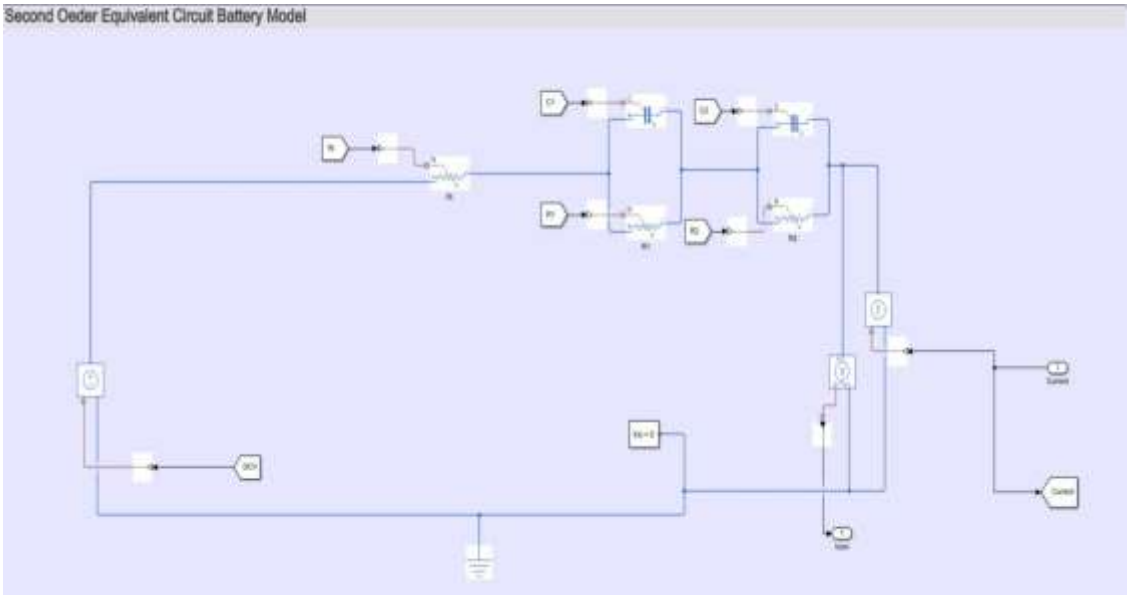

Figure 16 SOEC battery model - Matlab/Simulink

The HPPC characterisation tests conducted on the LTO battery cell is used dot capture the data for OCV at different stages during the experiment. The OCV data is recorded at the end of each rest phase after the high current charge after the discharge pulse is injected. The OCV recorded at this point also states that the voltage has attained a steady-state value (Locorotondo et al., 2018). The other parameters are calculated using the same HPPC characterisation tests results. The voltage response from the characterisation tests is recorded and it is used to calculated other parameters in the SOEC model.

The ohmic resistance value is observed and recorded from the instantaneous voltage drop immediately after the current pulse is applied. The initial period close to 0.1s, where the voltage drop is linear, is used to calculate the value of Ri. From Ohm's Law, Ri was calculated from equation 5. Here, the value of *V0* is recorded before the current pulse is applied (OCV) and *V1* is the measured voltage after a second resolution span, and I is the current pulse amplitude.

$$Ri = \frac{V0 - V1}{I} \tag{5}$$

The two RC parallel network values are based on time transients, as described in the equation below. As described earlier, the first RC network represents the fast voltage response dynamics, and the second RC network represents the slow voltage response dynamics. These transients are described in equation 6 and 7, respectively.

$$T_1 = R_1 C_1 \tag{6}$$

$$T_2 = R_2 C_2 \tag{7}$$

Thus, by using Kirchhoff's current lar in the first RC network, the current charging capacitor C1 must be equal to the current through resistor R1. Similarly, for the second RC network where t_3 and t_2 represent the starting and ending of the slow voltage process. Additionally, the values of R1 and R2 were calculated by employing Ohm's Law:

$$R1 = \frac{V1 - V2}{I} \tag{8}$$

$$R2 = \frac{V2 - V3}{I} \tag{9}$$

Here, the voltage values were calculated at the same points as the respective time transients, i.e., V_1, V_2, and V_3, calculated at time points t_1, t_2 and t_3, respectively. The values for capacitance were calculated by using the already estimated values and the equation is as follows:

$$C1 = \frac{\tau 1}{R1} \tag{10}$$

$$C2 = \frac{\tau 2}{R2} \tag{11}$$

Thus, the values estimated from the SOEC parameters were further used in simulating the battery voltage by using the below equation. The obtained result was compared with the results obtained from the laboratory experiments. The voltage equation is given below as follows:

$$V(t) = V_{OCV} + I(t)R_i + I(t)R_1\left(1 - e^{\left(-\frac{t}{t1}\right)}\right) + I(t)R_2\left(1 - e^{\left(-\frac{t}{t2}\right)}\right) \qquad (12)$$

The least-square curve fitting methodology is widely popular for any given data. It is used to understand and determine the position of a trend line for any time series. In this method, the mathematical relation is recognised in the time factor and other variables. The curve consisting of minimum deviations is regarded as the best fit in this methodology. Various measurements are combined to derive the parameters that specify the curve for the best fit (Molugaram & Rao, 2017a; Molugaram & Rao, 2017b; Nixon & Aguado, 2012). In Simscape, Matlab software uses the least square data fitting technique, which requires a parametric model related to the response data of the predictor data with one or more coefficients. The least-square curve fitting used in this thesis takes various variables into consideration, such as Ri_init, R1_init, R2_init, C1_init and C2_init. These values are the product of the HPPC characterisation test. The use of a lower bound and upper bound is also considered in the calculation. The equation below states the least square curve fit methodology:

$$min_{+}\|F(x,xdata) - ydata\|^{*} = min^{+}\Sigma\,(F(x, xdata) - ydata)^{*}$$

Here, the given input data is x-data and the observed output y-data, where x-data and y-data are matrices of the vectors. F(x, xdata) is matrix values of the same size as y-data. It also uses the lower and upper bound of the matrices. The lsqcurvefit provides a convenient and straightforward interface for data fitting problems. Rather than compute the sum of squares, lsqcurvefit requires the user-defined function to compute the *vector*-valued function

Figure 16 depicts the Simscape version SOEC model for LTO battery cell modelling. AS stated in the early section, it consists of six main components. Figure 16 illustrates

various elements used in the model recorded from the HPPC characterisation test. The two parallel networks required in this model needed to be parametrised using the HPPC tests records. Thus, the 10-sec pulse was divided into two more points; the first shows the short transient, whereas the second is used to indicate the longer transient and are represented by T1 and T2, respectively. The values determined from these two-time transients are used to estimate Ri, R1, R2, C1 and C2 using the above formulas from 1-5. The values obtained are fed to equation 6, thus simulating the voltage of the LTO battery cell. Calculated values at different SOC's and temperatures are then normalised using lsqcurvefit in Matlab, which provides a least-squares fitting methodology for non-linear data. The voltage response curve obtained from the HPPC characterization tests is illustrated in Figure 17 below:

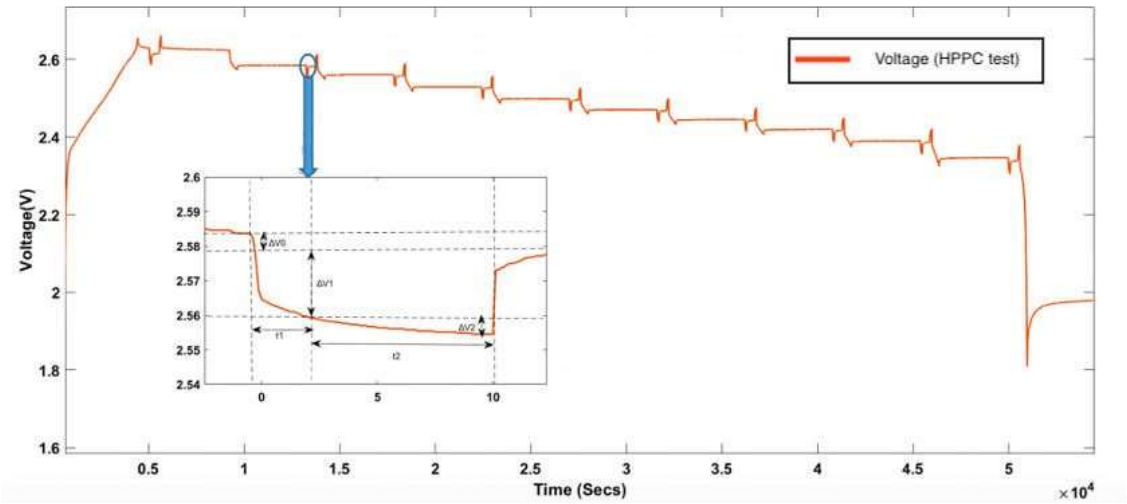

Figure 17 Voltage response

The parameter estimation required for the modelling technique was calculated as stated in the equations 5 – 12; the representation of these equations was performed in Simscape Matlab software. The result data collection from the HPPC experimental tests is imported into the Matlab software. Appendix A – HPPC test Data sorting imports this data from excel (.xls) files. The required data is sorted in different timeslots depending upon different breakpoints depicting various stages. Similarly, the data sorting for four operating temperatures is achieved in this code.

Appendix B – Parameter estimation 1 states this representation in Matlab software in a structured code. The code initially imports the required data from the excel (.xls) files; the OCV is calculated from this data at a designated point. The data from Appendix A – HPPC test Data sorting is used to calculate the initial five elements Ri, R1, R2, C1 and C2. The initial elements are calculated by using the slow and fast transient characteristics. The least square curve fitting methodology is used, which also takes the lower and upper bound into consideration (0 and 100 respectively). Thus, the values of Ri, R1, R2, C1 and C2 are calculated and sorted as per the requirement in Simulink software. Similarly, voltage, current and time span are sorted from the HPPC test data. The procedure is repeated for all four temperatures.

The data from Appendix B – Parameter estimation 1 is then loaded in Appendix C – Parameter estimation 2, where the results are sorted in various tables separately with respect to the operating temperatures. The result is loaded to the Simulink workspace required for the simulation.

Figure 18 depicts the evolution of the ECM parameters concerning time and SOC on a 3-dimensional plot. Figure 4 (a) represents the Ri of the cell pertaining to ΔV0 in the HPPC response curve. The Ri value is proportional to SOC and inversely proportional to temperature. Similarly, Figure 4 (b) and (c) illustrates short transient parameters of the RC branch network derived from the voltage (ΔV1). Figure 4 (d) and (e) represent the long transient parameters of the RC branch network and are derived from the voltage (ΔV2), which is assumed to describe the dynamics during the diffusion process of cell operation. The least-squares fitting methodology for non-linear data is used to calculate values at different SOCs and temperatures. OCV values decrease over time and are shown in Fig 4(f).

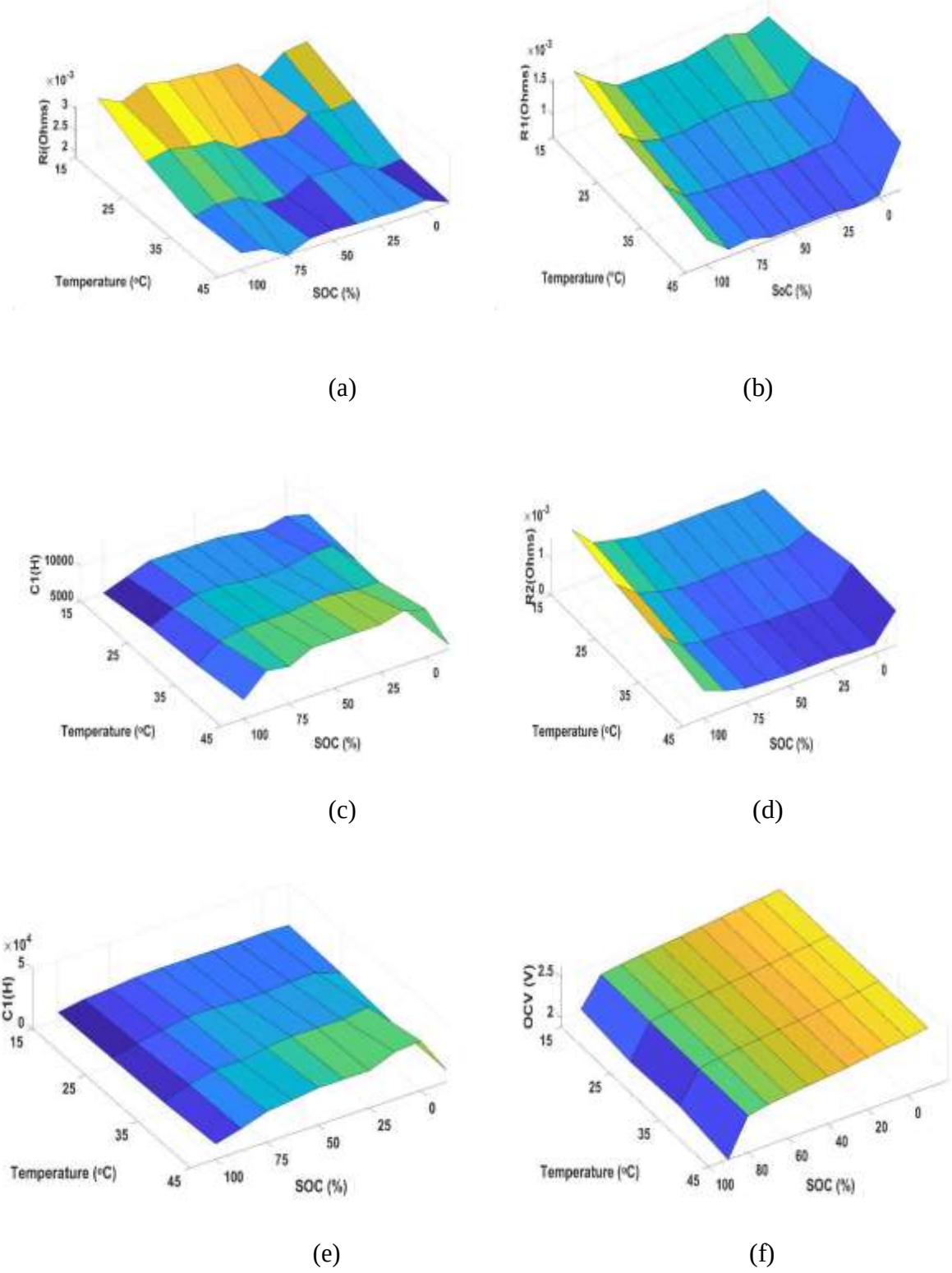

(a) (b)

(c) (d)

(e) (f)

Figure 18 ECM parameters at different SOC levels and temperatures

4.2 SOC estimation using the coulomb counting method

The next step in modelling the LTO battery cell includes the estimation of the SOC of the battery. It is one of the most important aspects of any BMS system to provide the SOC estimate. In grid systems, similar to the other battery operations, the BMS system is required to optimise the overall performance of the battery from time to time, which is used to determine the most optimal strategy for the application of the battery cell. Thus, SOC is calculated in different sections. As stated earlier, SOC estimation is the ratio of the current Ampere-Hour (Ah) to the total available Ampere-Hour (AH) at the initial condition (Ng et al., 2009).

Coulomb counting SOC estimation method

It is essential to have a precise SOC estimation as per the application's need in order to avoid unwanted interruptions in the system during the application, especially in the case of smart grid systems where precision and speed is essential. SOC estimation such as adaptive systems and direct measurements are not generally considered best suited due to the time requirement and low accuracy. Various factors affect the accuracy of the SOC estimation in the direct measurement system and. In contrast, adaptive systems are crucial estimation model for the future due to sophisticated accuracy levels but require sufficient training data for good precision. The book-estimation methodology is one of the best-suited models due to its simplistic design, flexibility and high accuracy (Guo & He, 2018; Ng et al., 2009)

The SOC is calculated by the coulomb counting/ampere-hour method in this thesis. This method generally measures the battery current and integrates the current overtime to estimate the SOC of the battery. This methodology is suitable for applications where higher precision is required as it is known for monitoring the rapid fluctuations in SOC. The coulomb counting method provides higher accuracy at minimal computation effort due to lower noise levels in the environment. The initial value of the SOC_0 is known at the time t_0, then the battery SOC at any specific time t can be calculated by using the

below formula (Chang, 2013; Guo & He, 2018; Jeon, Yun, & Bae, 2015; Zhao, L., Lin, & Chen, 2016):

$$SOC(t) = SOC(t-1) + \frac{I(t)}{Q_n}\,\Delta t \tag{13}$$

Several factors such as temperature, battery ageing, history of usage, initial SOC and cycle life all affect the precision of the coulomb counting methodology. If any initial errors occur in recording the initial current value I then the accuracy of this method is affected, causing more significant errors in estimation. Thus, the accuracy of the current measurement plays an important role in achieving higher accuracy in the coulomb counting method for SOC estimation (Attanayaka, Karunadasa, & Hemapala, 2019; Jeon et al., 2015; Ng et al., 2009). However, in this work, the initial SOC values and current measurements are provided by the experimentation with Neware BTS8000 cycler, which has high accuracy in measurements. Thus, the Coulomb counting method provides the least computational burden in SOC calculation and the highest prediction accuracy (Nemounehkhah et al., 2020). The representation of the coulomb counting method in the Simscape Matlab/Simulink software is illustrated in the Figure 19 below:

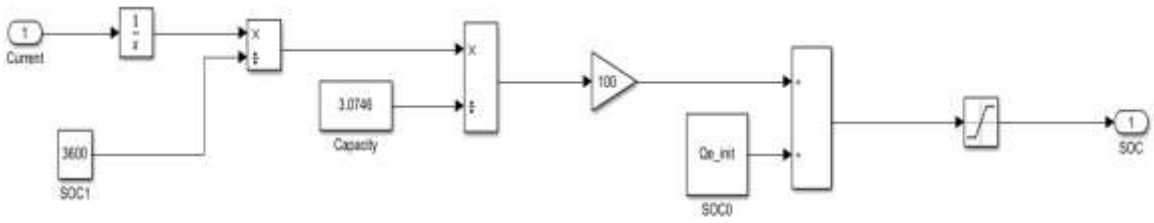

Figure 19 Coulomb counting SOC estimation method (Simscape Matlab/Simulink software)

As stated earlier, the input required for the coulomb counting method is current and SOC. Thus, the information is fed to the block from current to an integrator used in Simulink to give an output of the value of the integral of the input signal with respect to time. This is important as time span plays an important factor in this methodology. It is further fed ahead with a constant value and together, it is compared with the actual capacity of the LTO battery cell, which in this case is 3.7046 mAh. They are compared and calculated ahead with the nominal capacity Qe_init.

Furthermore, it is fed to a saturation block, giving an output signal with respect to the upper and lower bounds applied for the process. Thus, the SOC is estimated using the coulomb counting methodology. Figure 20 below illustrates the output of SOC estimation by coulomb counting:

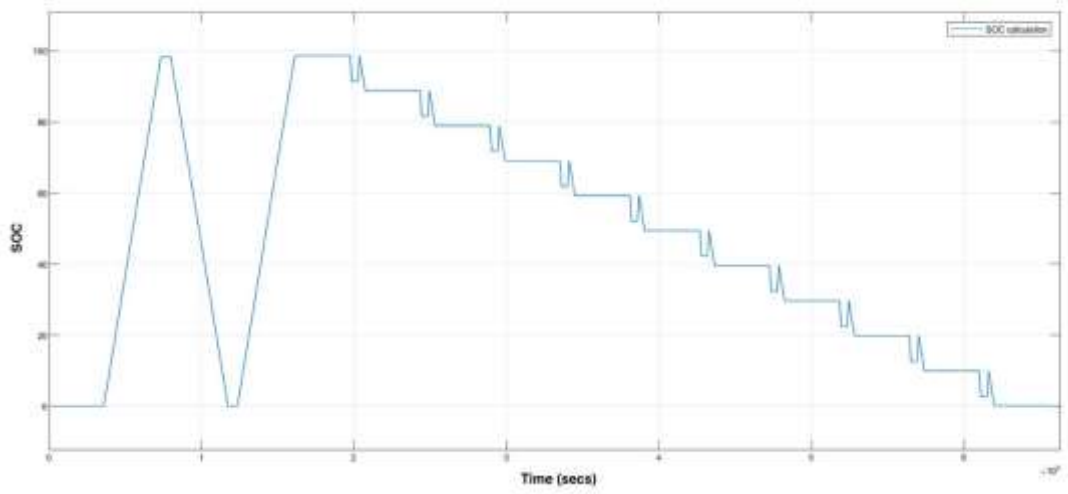

Figure 20 SOC estimation output (coulomb counting method)

The data analysed in the earlier step of modelling was stored and fed to the developed Simulink software model. Figure 21 below illustrates the primary model developed in Simscape Simulink:

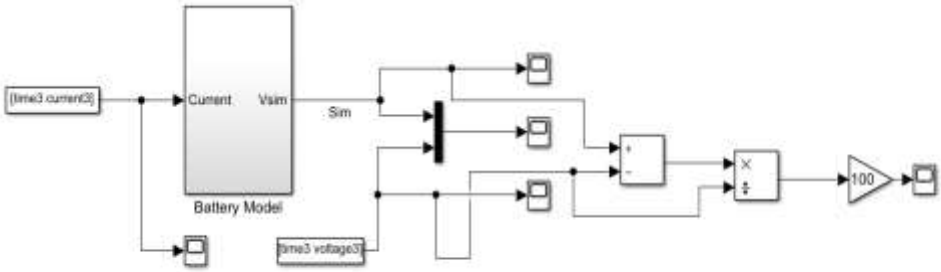

Figure 21 Battery model

The battery model consists of the SOC estimation model, battery parameter estimation model and the SOEC model. Figure 22 below illustrate the three developed models.

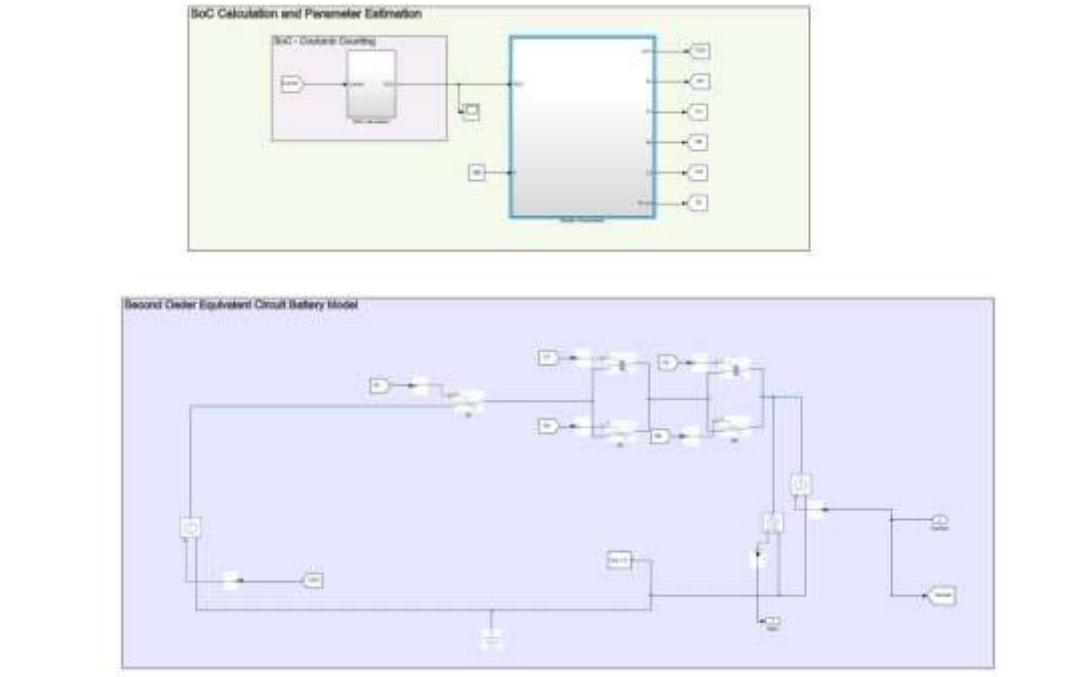

Figure 22 SOC estimation model, battery parameter estimation model and the SOEC model

The parameter estimation block uses the output from the SOC calculation block as well as the operating temperature. This block takes these two values and is used as breakpoints for the 2-D lookup table for different variables. The Lookup table uses the

Akima spline interpolation method. The below illustrates the parameter estimation block developed in Simscape Simulink software.

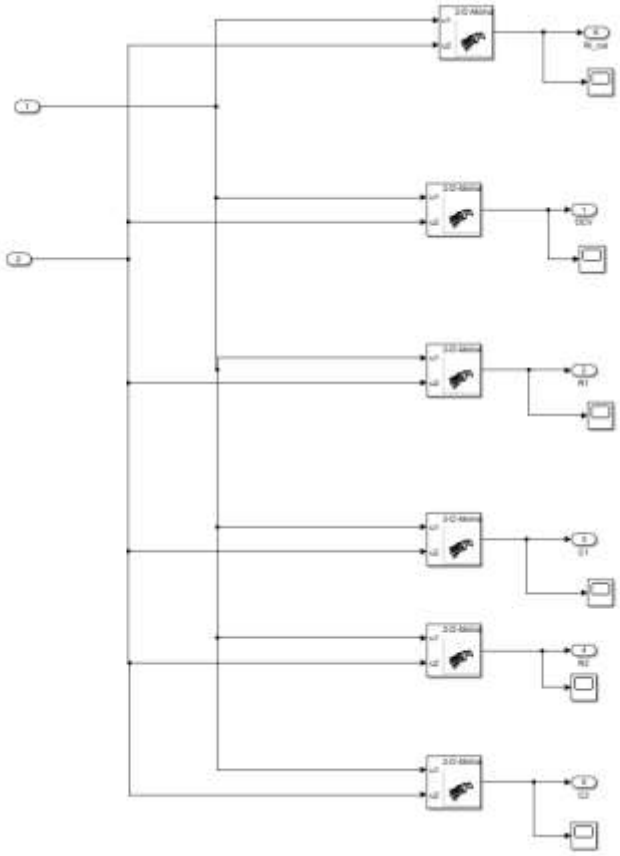

Figure 23 Parameter estimation block

The results of these models were recorded at different temperatures and SOC levels similar to that of the HPPC test results. The results from these two tests were superimposed to understand the difference in the results reported by the modelling of the battery cell. Similarly, the results between the tests were studied to find the error difference between these tests.

5 Results and Discussion

In this thesis, the proposed research of analysing the characteristics behaviour of the Toshiba LTO battery cell at different SOC levels and four different temperatures were achieved in this thesis. The characterisation was achieved by using experimental tests conducted in VEBIC labs at the University of Vaasa. The HPPC test was conducted for the characterisation of the battery cell. This was followed by modelling the battery cell to understand the behaviour and compare the modelling results with the experimental results of the battery.

For the characterisation of the battery, the hybrid pulse power characterisation tests were employed in the laboratories. The use of WEISS Technik weather chamber and Neware Battery cell testing equipment's were utilised for testing the battery cell. The HPPC test procedure was developed in a stepwise manner keeping various safety considerations as the top priority. The Toshiba LTO battery cell used in this experiment was a weather chamber at four different temperatures 15°C, 25°C, 35°C and 45°C. The LTO battery cells are known for their working even at lower temperatures. Thus, the lowest temperature decided for testing was 15°C. The characterisation test procedure carried out a specific script developed in the Neware battery cell testing equipment software, BTSDA-8000 model. The battery parameters such as open-circuit voltage, internal resistance and the power capability of the battery were recorded during the HPPC test at different SOC levels ranging from 0% to 100% at 10% interval. The measurements mentioned earlier were recorded during the discharging of the battery cell. The results from the characterisation tests were recorded and studied to understand the battery behaviour during the controlled situations. Various findings from the battery characterisation tests at different temperatures are shown below in Figure 24, Figure 25, Figure 26 and Figure 27:

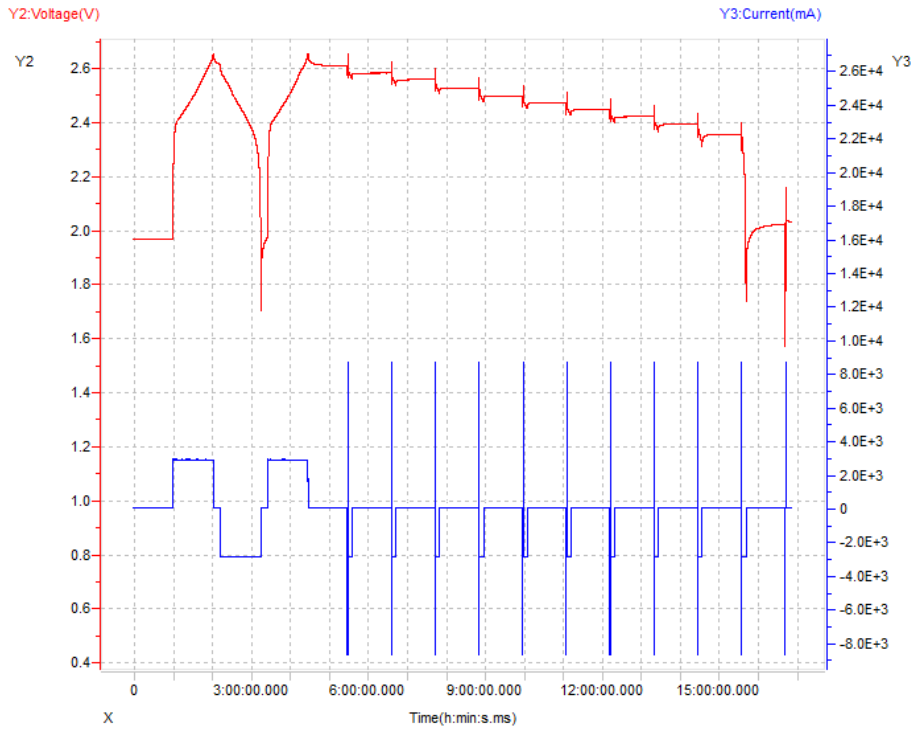

Figure 24 HPPC test results at 15°C

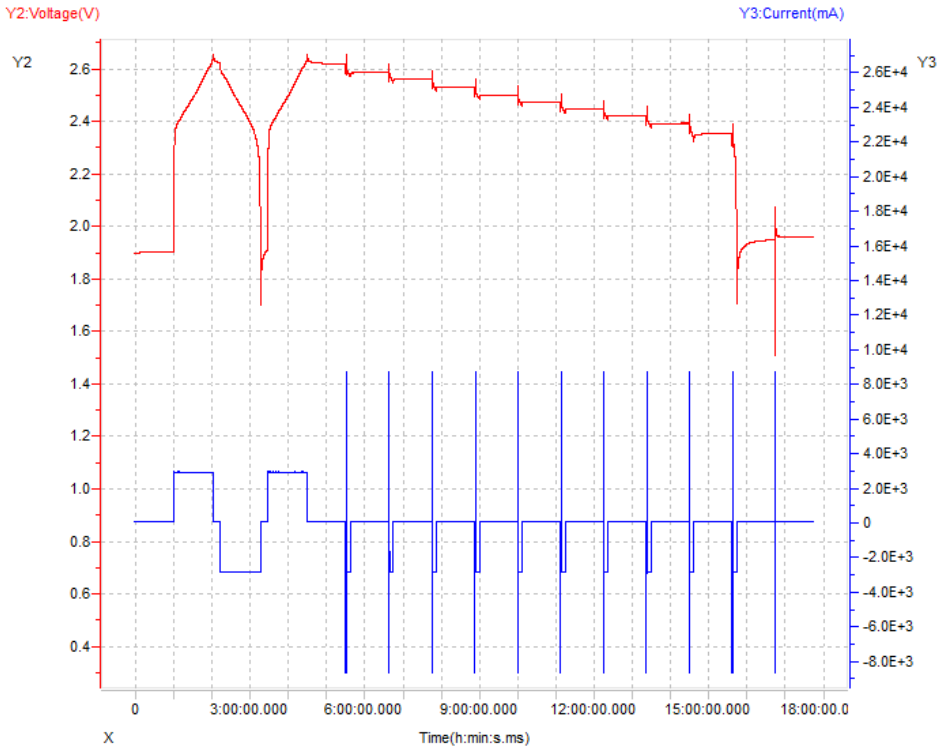

Figure 25 HPPC test results at 25°C

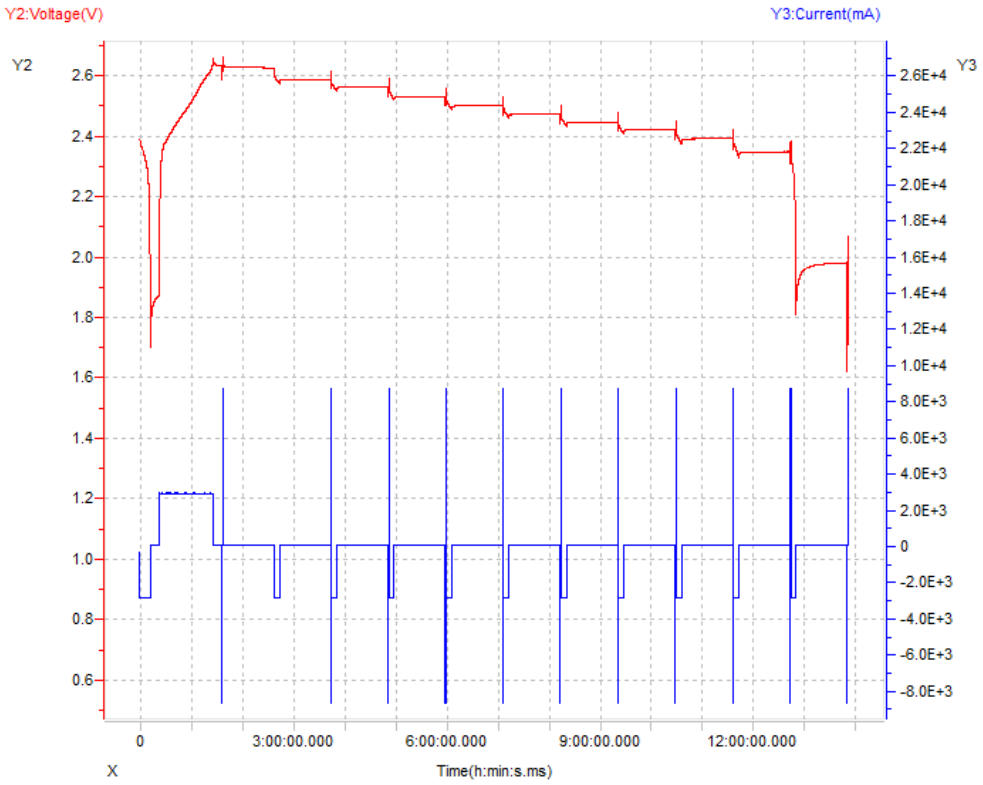

Figure 26 HPPC test results at 35°C

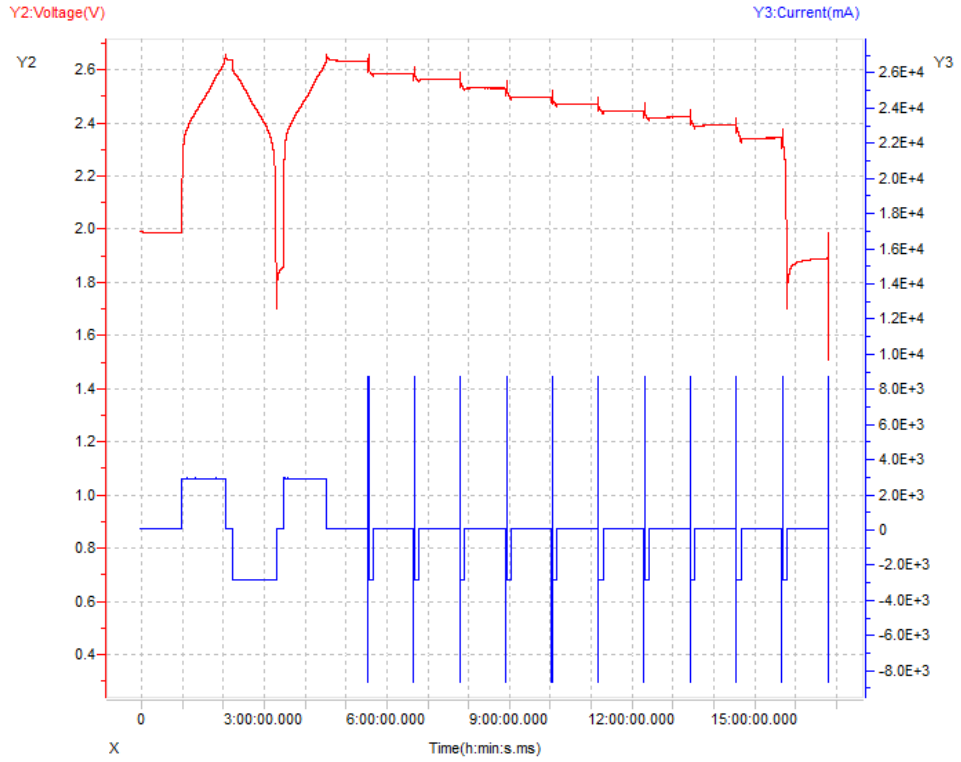

Figure 27 HPPC test results at 45°C

The above figures illustrate the HPPC test results at 15°C, 25°C, 35°C and 45°C using the same HPPC test script developed using Neware BTSDA-8000 model software. The script for 35°C varied slightly but did not have any effect on the outcome of the final readings. The HPPC test starting voltage was always reached at 100% SOC level, which was 2.6497 V. This value is then stepwise discharged by giving current pulses; the voltage value dropped slightly more in the experiments with higher temperatures compared to a lower temperature. This was a cumulative factor that affected the final temperature drop in the last SOC level across temperatures. Thus, the final voltage recorded at the end of each HPPC test, voltage recordings were higher at lower temperatures. In contrast, at that higher temperatures, the voltage readings were comparatively lower.

The HPPC test characterisation experiments recordings were used in developing the proposed SOEC models. These models were developed, and the battery behaviour was recorded from the models. Both results of the experimental tests and modelled recordings were compared to study the accuracy of the model.

The proposed SOC estimation was developed from the parameters estimated from the HPPC characterization tests. The SOC estimation was successfully performed using the coulomb counting method. In the initial stage of the coulomb counting method, the initial value of the SOC_0 is known at the time t_0, then the battery SOC at any specific time t is calculated.

The proposed SOEC model was developed in this thesis. This modelling technique required various electrical parameters which were recorded from the HPPC test experiments. The SOEC model was developed using Simscape Matlab/Simulink software. The estimation of the parameters was conducted using Matlab software consisting of parameter estimation mathematical algorithms — the recorded BTSDA software data is used as the input for parameter estimation. The imported data was analysed, and data sorting was implemented to store the required data. The data sorting procedure is important to reduce the time consumed in the analysis. This data was fed as the initial

data for certain parameters, which were further calculated. This sorted data was in non-linear form and was normalised using the least square curve fit method, '*lsqcurvefit*' in Simscape Matlab software. The output of this is stored to be used in the Simulink software.

The validation of the SOEC model is achieved with the extracted parameters from the optimisation script. These parameters are used to simulate the cell voltage response for the LTO battery cell along with the HPPC test profile used for extraction of parameters. The simulated voltage response at 35°C is shown in Figure 30 below. The validation of the proposed model is validated from Figure 30, as the simulated voltage curve almost superimposes the experimental curve. Figure 34 illustrates the error percentage for the model at 35°C. The overall modelling error observed is approximately less than 2% for the range of 10% to 100% SOC levels. The model response is quite poor at SOC levels below 10%, with a model error percentage ranging around 5%; this is due to the abrupt behaviour of battery cells at lower SOC levels and exponential voltage changes during charge/discharge. Similar results were observed at different temperatures, i.e., 15°C, 25°C and 45°C represented in Figure 32, Figure 33 and Figure 35 repectively.

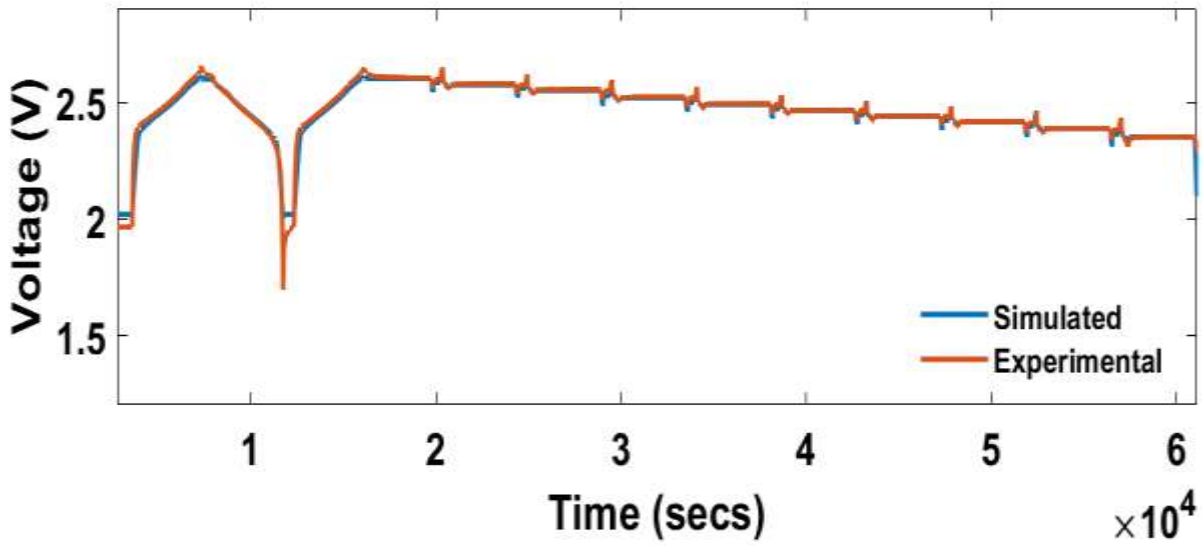

Figure 28 SOEC model performance in comparison with the experimental curve at 15°C

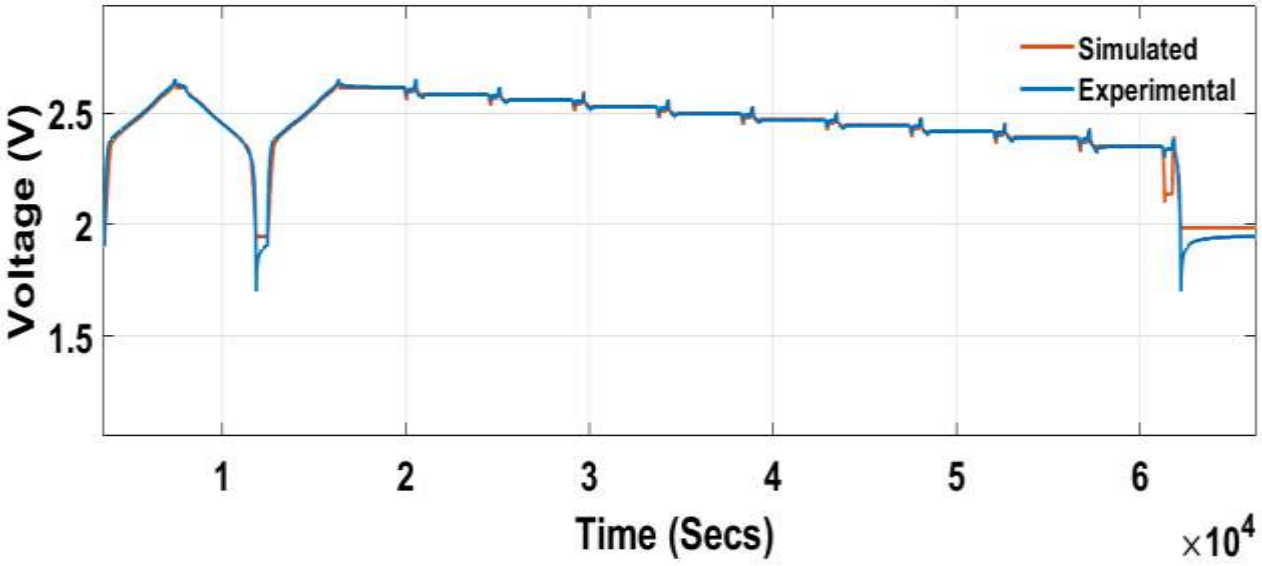

Figure 29 SOEC model performance in comparison with the experimental curve at 25°C

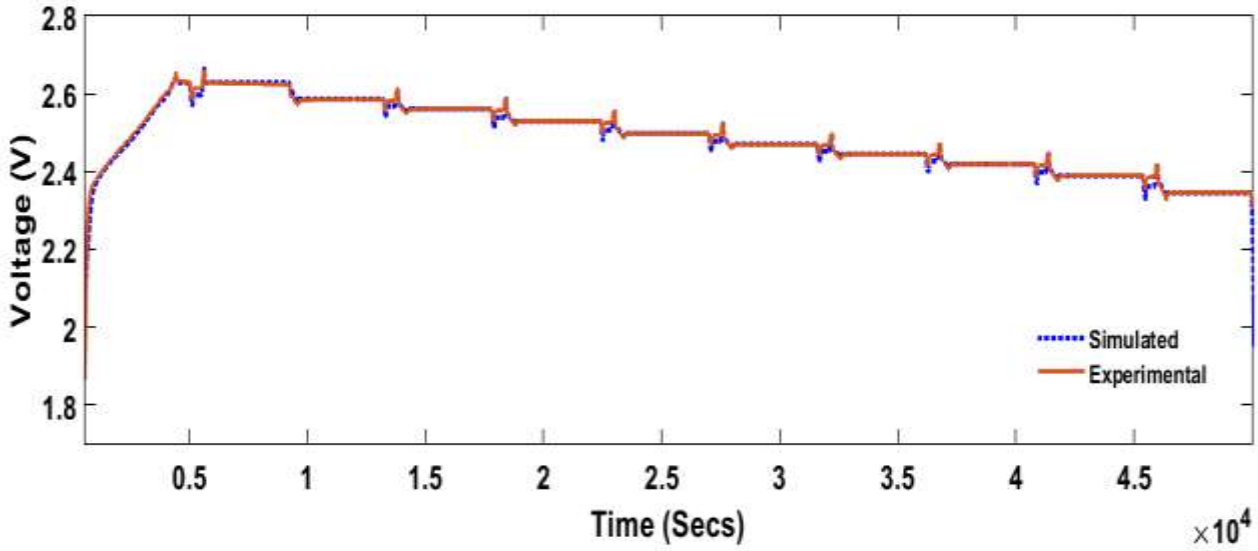

Figure 30 SOEC model performance in comparison with the experimental curve at 35°C

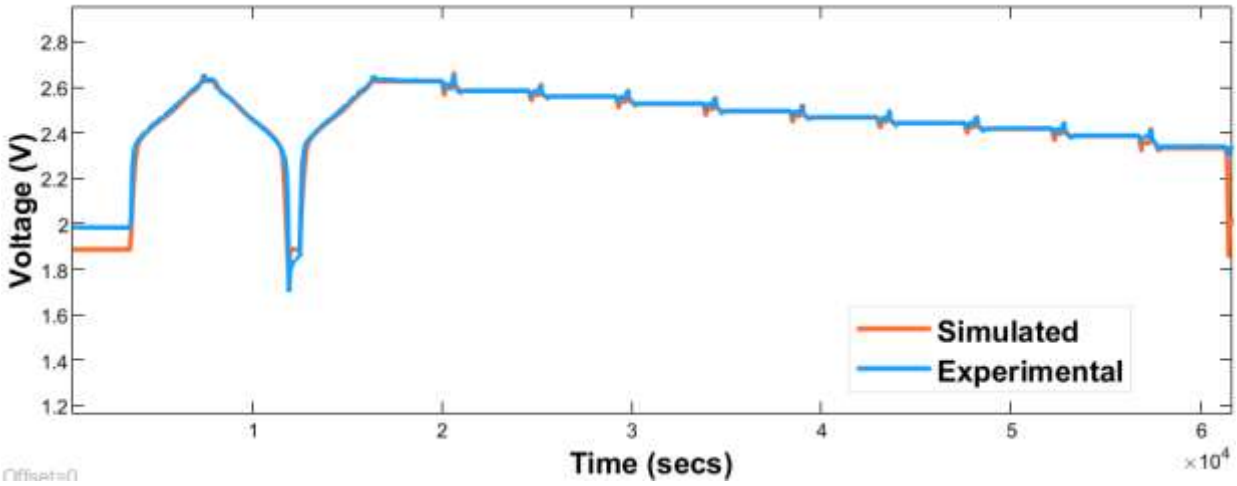

Figure 31 SOEC model performance in comparison with the experimental curve at 45°C

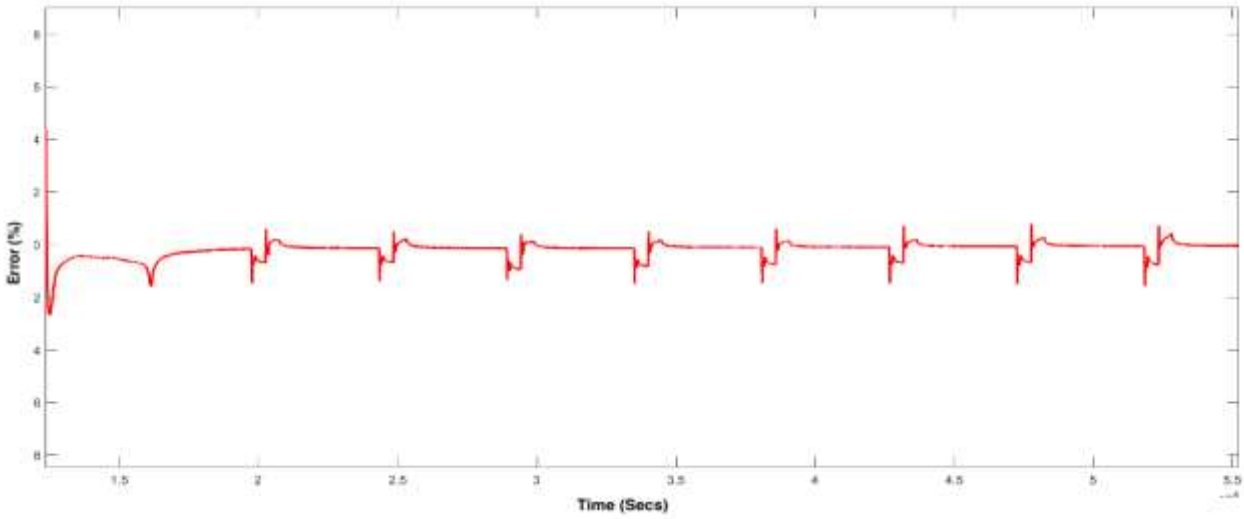

Figure 32 Comparison of error percentage at 15°C

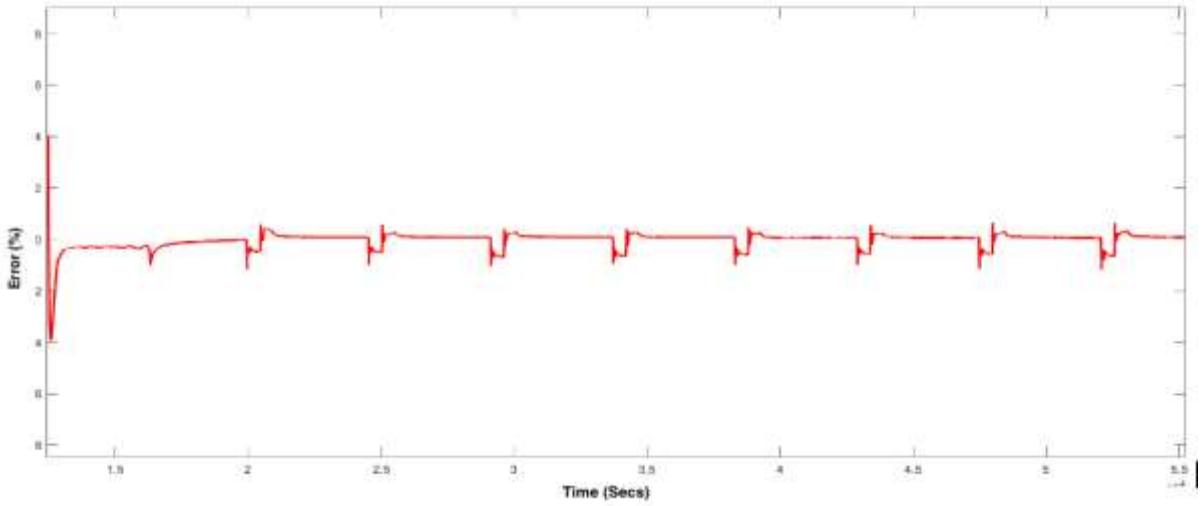

Figure 33 Comparison of error percentage at 25°C

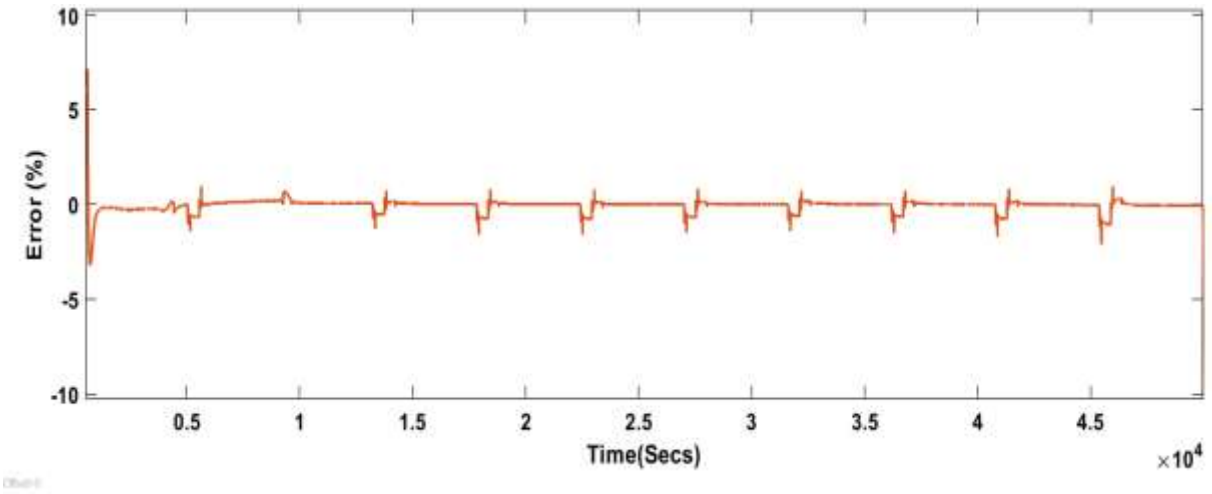

Figure 34 Comparison of error percentage at 35°C

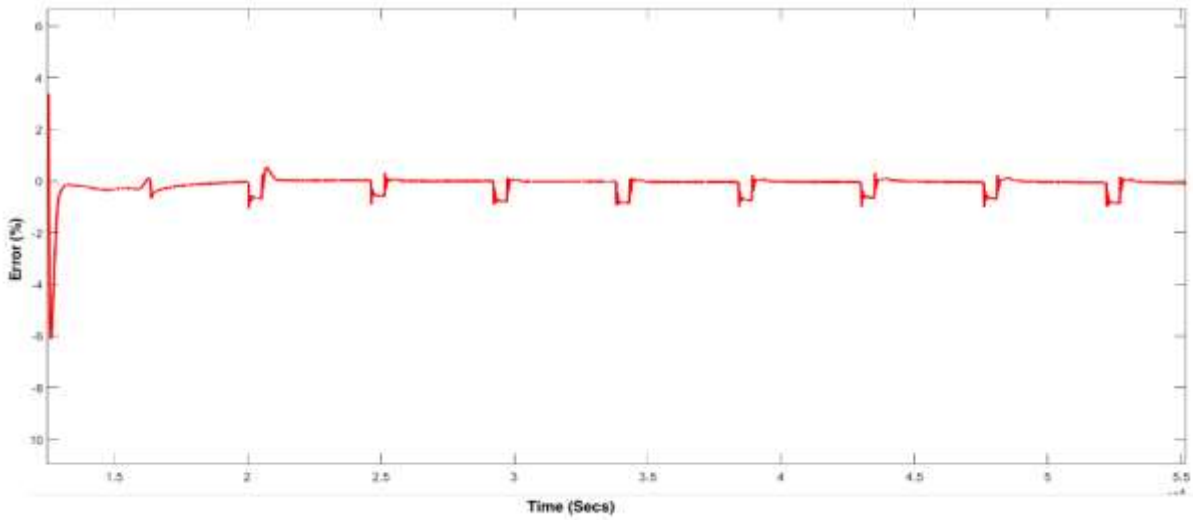

Figure 35 Comparison of error percentage at 45°C

6 Conclusion

The ever-increasing GHG's need for renewable energy sources has become evident. Energy storage systems are seen as the future and Li-ion batteries will play a vital role. The recent development in Li-ion batteries has seen various types of batteries in the market. LTO batteries will play an influential role in land-based smart grid applications due to their versatility in design and features. However, it is necessary to understand and observe battery behaviour at different conditions due to their non-linear behaviour.

This study focuses on the LTO battery cell and its behaviour under controlled conditions. The study stated the battery behaviour is influenced by various aspects but mainly by the operating temperature and SOC level. The battery behaviour of an LTO battery cell at different temperatures (15°C, 25°C, 35°C and 45°C) and SOC levels (0% - 100%) were studied. The thesis also aims to establish an extensive SOEC model for the LTO battery cell to observe the parameters affecting battery behaviour. Through comprehensive literature, including the state of the art of Li-ion batteries have been evaluated. Characterization test experiments procedure were developed and conducted in the laboratory on the LTO battery cell. Based on the characterization tests, the SOEC battery model was developed, which can be used for land-based grid applications as well as other similar applications.

The results from the simulations models were validated by comparing them with the experimental curves. The comparison between the simulation and experimental curves show extraordinary results as the error percentage of these two results was approximately less than 2% for the majority of the model. At lower SOC levels from 10% - 0% observed higher error percentage around 5%. The SOEC model structure could be improvised for lower SOC levels and other parameter estimation methods could be a possible solution for increasing the accuracy and model performance. Thus, improving the existing LTO battery cell model forms a basis for future studies.

References

Aalborg Universitet Lifetime Models for Lithium-ion Batteries used in Virtual Power Plant Applications Stroe, Daniel Ioan-defence-by- daniel-ioan-stroe-on-lifetime-models-for-lithium-ion-batteries-used-in-virtual-power-plant-applications.cid131015

Abdi, H., Mohammadi-ivatloo, B., Javadi, S., Khodaei, A. R., & Dehnavi, E. (2017). Chapter 7 - Energy Storage Systems. In G. B. Gharehpetian, & S. M. Mousavi Agah (Eds.), Distributed Generation Systems (pp. 333-368). Butterworth-Heinemann. https://doi.org/10.1016/B978-0-12-804208-3.00007-8

Adamec, J., Danko, M., Taraba, M., & Drgona, P. (2019). Analysis of selected energy storage for electric vehicle on the lithium based. Transportation Research Procedia, 40, 127-131.

Allen, M., Antwi-Agyei, P., Aragon-Durand, F., Babiker, M., Bertoldi, P., Bind, M., Brown, S., Buckeridge, M., Camilloni, I., Cartwright, A., Cramer, W., Dasgupta, P., Diedhiou, A., Djalante, R., Dong, W., Ebi, K. L., Engelbrecht, F., Fifita, S., Ford, J., . . . Zickfeld, K. (2019). Technical Summary: Global warming of 1.5°C. An IPCC Special Report on the impacts of global warming of 1.5°C above pre-industrial levels and related global greenhouse gas emission pathways, in the context of strengthening the global response to the threat of climate change, sustainable development, and efforts to eradicate poverty. Intergovernmental Panel on Climate Change.

Aristizábal, A. J., Herrera, J., Castañeda, M., Zapata, S., Ospina, D., & Banguero, E. (2019). A new methodology to model and simulate microgrids operating in low latitude countries. Energy Procedia, 157, 825-836.

Arunachala, R. (2018). Influence of Cell Size on Performance and Lifetime of Lithium-Ion Batteries. Influence of Cell Size on Performance and Lifetime of Lithium-Ion Batteries,

ASIAN DEVELOPMENT BANK. (2018). HANDBOOK ON BATTERY ENERGY STORAGE SYSTEM. ASIAN DEVELOPMENT BANK.

Attanayaka, A., Karunadasa, J. P., & Hemapala, K. (2019). Estimation of state of charge for lithium-ion batteries—A Review. AIMS Energy, 7(2), 186-210.

Baba, A., & Adachi, S. (2014). SOC estimation of HEV/EV battery using series Kalman filter. Electrical Engineering in Japan, 187(2), 53-62.

Baccouche, I., Jemmali, S., Mlayah, A., Manai, B., & Amara, N. E. B. (2018). Implementation of an improved Coulomb-counting algorithm based on a piecewise SOC-OCV relationship for SOC estimation of li-IonBattery. arXiv Preprint arXiv:1803.10654,

Barré, A., Deguilhem, B., Grolleau, S., Gérard, M., Suard, F., & Riu, D. (2013). A review on lithium-ion battery ageing mechanisms and estimations for automotive applications. Journal of Power Sources, 241, 680-689.

Belt, J. R. (2010). Battery test manual for plug-in hybrid electric vehicles. Battery Test Manual for Plug-in Hybrid Electric Vehicles,

Buchmann, I., & Cadex, E. I. (2001). Batteries in a Portable World: A Handbook on Rechargeable Batteries for Non-engineers. Cadex Electronics.

Burke, A., & Miller, M. (2009). Performance characteristics of lithium-ion batteries of various chemistries for plug-in hybrid vehicles.

Burke, A., Miller, M., Burke, A., & Miller, M.UC Davis Recent Work Title Performance Characteristics of Lithium-ion Batteries of Various Chemistries for Plug-in Hybrid Vehicles Publication Date Performance Characteristics of Lithium-ion Batteries of Various Chemistries for Plug-in Hybrid Vehicles

Bustos, R., Siddique, A. R. M., Cheema, T., Gadsden, S. A., & Mahmud, S. (2018). State of charge and parameter estimation of electric vehicle batteries.

Ceder, G., Doyle, M., Arora, P., & Fuentes, Y. (2002). Computational Modeling and Simulation for Rechargeable Batteries. MRS Bulletin, 27(8), 619-623. 10.1557/mrs2002.198

Chang, W. (2013). The state of charge estimating methods for battery: A review. International Scholarly Research Notices, 2013

Chauhan, P. J., Reddy, B. D., Bhandari, S., & Panda, S. K. (2018). Battery energy storage for seamless transitions of wind generator in standalone microgrid. IEEE Transactions on Industry Applications, 55(1), 69-77.

Chen, T., Jin, Y., Lv, H., Yang, A., Liu, M., Chen, B., Xie, Y., & Chen, Q. (2020). Applications of lithium-ion batteries in grid-scale energy storage systems. Transactions of Tianjin University, 26(3), 208-217.

Danko, M., Adamec, J., Taraba, M., & Drgona, P. (2019). Overview of batteries State of Charge estimation methods. Transportation Research Procedia, 40, 186-192. https://doi.org/10.1016/j.trpro.2019.07.029

Dees, D. W., Battaglia, V. S., & Bélanger, A. (2002). Electrochemical modeling of lithium polymer batteries. Journal of Power Sources, 110(2), 310-320.

Doeff, M. (2012). Batteries: Overview of Battery Cathodes. (pp. 709-739)

Dong, H., Li, S., Liu, H., Mei, J., Liu, H., & Liu, G. (2019). Facile synthesis and electrochemical properties of LiNi0.8Co0.15Al0.05O2 with enlarged exposed active planes for Li-ion batteries. Ionics, 25(2), 827-834. 10.1007/s11581-018-2620-5

Doyle, M., & Newman, J. (1995). The use of mathematical modeling in the design of lithium/polymer battery systems. Electrochimica Acta, 40(13-14), 2191-2196.

E. Chemali, M. Preindl, P. Malysz, & A. Emadi. (2016). Electrochemical and Electrostatic Energy Storage and Management Systems for Electric Drive Vehicles: State-of-the-Art Review and Future Trends10.1109/JESTPE.2016.2566583

Eddahech, A., Briat, O., & Vinassa, J. (2015). Performance comparison of four lithium–ion battery technologies under calendar aging. Energy, 84, 542-550. https://doi.org/10.1016/j.energy.2015.03.019

Gao, Y., Zhang, X., Yang, J., & Guo, B. (2018). Estimation of state-of-charge and state-of-health for lithium-ion degraded battery considering side reactions. Journal of the Electrochemical Society, 165(16), A4018.

Garcia, P., Fernandez, L. M., Garcia, C. A., & Jurado, F. (2009). Energy management system of fuel-cell-battery hybrid tramway. IEEE Transactions on Industrial Electronics, 57(12), 4013-4023.

Guo, D., & He, L. (2018). A novel algorithm for soc using simple iteration and coulomb counting method. Paper presented at the 2018 IEEE Student Conference on Electric Machines and Systems, 1-4.

Hannan, M. A., Hoque, M. M., Mohamed, A., & Ayob, A. (2017). Review of energy storage systems for electric vehicle applications: Issues and challenges. Renewable and Sustainable Energy Reviews, 69, 771-789. https://doi.org/10.1016/j.rser.2016.11.171

Haq, I. N., Leksono, E., Iqbal, M., Sodami, F. N., Kurniadi, D., & Yuliarto, B. (2014). Development of battery management system for cell monitoring and protection. Paper presented at the 2014 International Conference on Electrical Engineering and Computer Science (ICEECS), 203-208.

Harris, W. S. (1958). Lawrence Berkeley National Laboratory Recent Work Title ELECTROCHEMICAL STUDIES IN CYCLIC ESTERS Permalink https://escholarship.org/uc/item/74t234gs Publication Date

Hinz, H. (2019). Comparison of Lithium-Ion battery models for simulating storage systems in distributed power generation. Inventions, 4(3), 41.

How Does a Lithium-ion Battery Work? (2017). U.S. Department of Energy. https://www.energy.gov/eere/articles/how-does-lithium-ion-battery-

work#:~:text=The%20electrolyte%20carries%20positively%20charged,at%20the%20positive%20current%20collector.&text=The%20separator%20blocks%20the%20flow%20of%20electrons%20inside%20the%20battery.

Hua, X., Zhang, C., & Offer, G. (2021). Finding a better fit for lithium ion batteries: A simple, novel, load dependent, modified equivalent circuit model and parameterization method. Journal of Power Sources, 484, 229117.

Huang, P., Wang, Q., Li, K., Ping, P., & Sun, J. (2015). The combustion behavior of large scale lithium titanate battery. Scientific Reports, 5(1), 7788. 10.1038/srep07788

Hussein, A. A., & Batarseh, I. (2011). An overview of generic battery models. Paper presented at the 2011 IEEE Power and Energy Society General Meeting, 1-6.

Ibrahim, H., Ilinca, A., & Perron, J. (2008a). Energy storage systems—Characteristics and comparisons. Renewable and Sustainable Energy Reviews, 12(5), 1221-1250.

Ibrahim, H., Ilinca, A., & Perron, J. (2008b). Energy storage systems—Characteristics and comparisons. Renewable and Sustainable Energy Reviews, 12(5), 1221-1250.

Jeon, S., Yun, J., & Bae, S. (2015). Comparative study on the battery state-of-charge estimation method. Indian Journal of Science and Technology, 8(26), 1-6.

Keil, P., & Jossen, A. (2016). Charging protocols for lithium-ion batteries and their impact on cycle life—An experimental study with different 18650 high-power cells. Journal of Energy Storage, 6, 125-141.

Kurzweil, P. (2010). Gaston Planté and his invention of the lead–acid battery—The genesis of the first practical rechargeable battery. Journal of Power Sources, 195(14), 4424-4434. https://doi.org/10.1016/j.jpowsour.2009.12.126

Lee, J., Lee, J., Nam, O., Kim, J., Cho, B. H., Yun, H., Choi, S., Kim, K., Kim, J. H., & Jun, S. (2006). Modeling and real time estimation of lumped equivalent circuit model of a lithium ion battery. Paper presented at the 2006 12th International Power Electronics and Motion Control Conference, 1536-1540.

LG Chem RESU HV. Battery test centre. https://batterytestcentre.com.au/batteries/lg-chem-resu-hv/

Li, S., He, H., Su, C., & Zhao, P. (2020). Data driven battery modeling and management method with aging phenomenon considered. Applied Energy, 275, 115340.

Linden, D. (1995). Handbook of batteries. Paper presented at the Fuel and Energy Abstracts, , 4(36) 265.

Locorotondo, E., Berzi, L., Platz, R., Nuffer, J., & Rauschenbach, M. (2018). EUROPEAN COMMISSION Horizon 2020 GV-07-2017 GA# 769506.

Madani, S. S., Schaltz, E., & Knudsen Kær, S. (2019). An electrical equivalent circuit model of a lithium titanate oxide battery. Batteries, 5(1), 31.

Manthiram, A. (2020). A reflection on lithium-ion battery cathode chemistry. Nature Communications, 11(1), 1550. 10.1038/s41467-020-15355-0

Manthiram, A., Muraliganth, T., Yamaki, J., & Tobishima, S. (2011). Lithium Intercalation Cathode Materials for Lithium-Ion Batteries; Rechargeable Lithium Anodeshttps://doi.org/10.1002/9783527637188.ch12; https://doi.org/10.1002/9783527637188.ch13

Manwell, J. F., & McGowan, J. G. (1993). Lead acid battery storage model for hybrid energy systems. Solar Energy, 50(5), 399-405.

Meng, J., Luo, G., Ricco, M., Swierczynski, M., Stroe, D., & Teodorescu, R. (2018a). Overview of lithium-ion battery modeling methods for state-of-charge estimation in electrical vehicles. Applied Sciences, 8(5), 659.

Meng, J., Luo, G., Ricco, M., Swierczynski, M., Stroe, D., & Teodorescu, R. (2018b). Overview of lithium-ion battery modeling methods for state-of-charge estimation in electrical vehicles. Applied Sciences, 8(5), 659.

Meng, J., Luo, G., Ricco, M., Swierczynski, M., Stroe, D., & Teodorescu, R. (2018c). Overview of Lithium-Ion Battery Modeling Methods for State-of-Charge Estimation in Electrical Vehicles10.3390/app8050659

Mishra, A., Mehta, A., Basu, S., Malode, S. J., Shetti, N. P., Shukla, S. S., Nadagouda, M. N., & Aminabhavi, T. M. (2018). Electrode materials for lithium-ion batteries. Materials Science for Energy Technologies, 1(2), 182-187. https://doi.org/10.1016/j.mset.2018.08.001

Molugaram, K., & Rao, G. S. (2017a). Chapter 12 - Analysis of Time Series. In K. Molugaram, & G. S. Rao (Eds.), Statistical Techniques for Transportation Engineering (pp. 463-489). Butterworth-Heinemann. https://doi.org/10.1016/B978-0-12-811555-8.00012-X

Molugaram, K., & Rao, G. S. (2017b). Chapter 5 - Curve Fitting. In K. Molugaram, & G. S. Rao (Eds.), Statistical Techniques for Transportation Engineering (pp. 281-292). Butterworth-Heinemann. https://doi.org/10.1016/B978-0-12-811555-8.00005-2

Moore, S., & Eshani, M. (1996). An empirically based electrosource horizon lead-acid battery model. SAE Transactions, , 421-424.

Narayan, A. (2017). State and parametric estimation of li-ion batteries in electrified vehicles.

Nemounehkhah, B., Faranda, R., Akkala, K., Hafezi, H., Parthasarathy, C., & Laaksonen, H. (2020). Comparison and evaluation of state of charge estimation methods for a verified battery model. Paper presented at the 2020 International Conference on Smart Energy Systems and Technologies (SEST), 1-6.

Ng, K. S., Moo, C., Chen, Y., & Hsieh, Y. (2009). Enhanced coulomb counting method for estimating state-of-charge and state-of-health of lithium-ion batteries. Applied Energy, 86(9), 1506-1511. https://doi.org/10.1016/j.apenergy.2008.11.021

Ng, K., Huang, Y., Moo, C., & Hsieh, Y. (2009). An enhanced coulomb counting method for estimating state-of-charge and state-of-health of lead-acid batteries. Paper

presented at the INTELEC 2009-31st International Telecommunications Energy Conference, 1-5.

Nitta, N., Wu, F., Lee, J. T., & Yushin, G. (2015). Li-ion battery materials: present and future. Materials Today (Kidlington, England), 18(5), 252-264. 10.1016/j.mattod.2014.10.040

Nixon, M. S., & Aguado, A. S. (2012). Chapter 11 - Appendix 2: Least squares analysis. In M. S. Nixon, & A. S. Aguado (Eds.), Feature Extraction & Image Processing for Computer Vision (Third Edition) (pp. 519-523). Academic Press. https://doi.org/10.1016/B978-0-12-396549-3.00017-3

Novaes Neto, N., Madnick, S., de Paula, M. G., & Malara Borges, N. (2020). A Case Study of the Capital One Data Breach. Stuart E.and Moraes G.De Paula, Anchises and Malara Borges, Natasha, A Case Study of the Capital One Data Breach (January 1, 2020),

Olabi, A. G. (2017). Renewable energy and energy storage systems. Renewable Energy and Energy Storage Systems,

Parthasarathy, C., Hafezi, H., & Laaksonen, H. (2020). Lithium-ion BESS Integration for Smart Grid Applications-ECM Modelling Approach. Paper presented at the 2020 IEEE Power & Energy Society Innovative Smart Grid Technologies Conference (ISGT), 1-5.

Parthasarathy, C., Thanagasundaram, S., & Jet, T. K. (2016). Study of applied pressure on open circuit characteristics and capacity of lithium polymer pouch cells. Paper presented at the 2016 Asian Conference on Energy, Power and Transportation Electrification (ACEPT), 1-6.

Pattipati, B., Sankavaram, C., & Pattipati, K. (2011). System identification and estimation framework for pivotal automotive battery management system characteristics. IEEE Transactions on Systems, Man, and Cybernetics, Part C (Applications and Reviews), 41(6), 869-884.

Purwanto, A., Yudha, C. S., Ubaidillah, U., Widiyandari, H., Ogi, T., & Haerudin, H. (2018). NCA cathode material: synthesis methods and performance enhancement efforts. Materials Research Express, 5(12), 122001. 10.1088/2053-1591/aae167

Reddy, M. V., Mauger, A., Julien, C. M., Paolella, A., & Zaghib, K. (2020). Brief History of Early Lithium-Battery Development. Materials, 13(8), 1884. 10.3390/ma13081884

Samadani, E., Lo, J., Fowler, M., Fraser, R. A., & Gimenez, L. (2013). Impact of Temperature on the A123 Li-Ion Battery Performance and Hybrid Electric Vehicle Range. Impact of Temperature on the A123 Li-Ion Battery Performance and Hybrid Electric Vehicle Range,

Scrosati, B. (2011). History of lithium batteries. Journal of Solid State Electrochemistry, 15(7), 1623-1630. 10.1007/s10008-011-1386-8

Scrosati, B., Garche, J., & Tillmetz, W. (2015a). Advances in battery technologies for electric vehicles. Woodhead Publishing.

Scrosati, B., Garche, J., & Tillmetz, W. (2015b). Advances in battery technologies for electric vehicles. Woodhead Publishing.

Spotnitz Robert. (2005). Battery Modeling. The Electrochemical Society Interface, 14

Stroe, A. (2018). Analysis of performance and degradation for Lithium titanate oxide batteries.

Stroe, A., Meng, J., Stroe, D., Świerczyński, M., Teodorescu, R., & Kær, S. K. (2018). Influence of Battery Parametric Uncertainties on the State-of-Charge Estimation of Lithium Titanate Oxide-Based Batteries. Energies, 11(4), 795.

Stroe, D. I. (2014). Lifetime models for Lithium-ion batteries used in virtual power plant applications.

Stroe, D., Knap, V., Swierczynski, M., Stroe, A., & Teodorescu, R. (2016). Operation of a grid-connected lithium-ion battery energy storage system for primary frequency

regulation: A battery lifetime perspective. IEEE Transactions on Industry Applications, 53(1), 430-438.

Sundén, B. (2019). Chapter 6 - Thermal management of batteries. In B. Sundén (Ed.), Hydrogen, Batteries and Fuel Cells (pp. 93-110). Academic Press. https://doi.org/10.1016/B978-0-12-816950-6.00006-3

Tariq, M., Maswood, A. I., Gajanayake, C. J., & Gupta, A. K. (2018). Modeling and integration of a lithium-ion battery energy storage system with the more electric aircraft 270 V DC power distribution architecture. Ieee Access, 6, 41785-41802.

Tesla Powerwall. Battery test centre. https://batterytestcentre.com.au/batteries/tesla-powerwall/

Thanagasundram, S., Arunachala, R., Makinejad, K., Teutsch, T., & Jossen, A. (2012a). A cell level model for battery simulation. Paper presented at the European Electric Vehicle Congress, 1-13.

Thanagasundram, S., Arunachala, R., Makinejad, K., Teutsch, T., & Jossen, A. (2012b). A cell level model for battery simulation. Paper presented at the European Electric Vehicle Congress, 1-13.

Tomasov, M., Kajanova, M., Bracinik, P., & Motyka, D. (2019). Overview of battery models for sustainable power and transport applications. Transportation Research Procedia, 40, 548-555.

Waag, W., Fleischer, C., & Sauer, D. U. (2014). Critical review of the methods for monitoring of lithium-ion batteries in electric and hybrid vehicles. Journal of Power Sources, 258, 321-339. https://doi.org/10.1016/j.jpowsour.2014.02.064

Wang, Q., Jiang, B., Li, B., & Yan, Y. (2016). A critical review of thermal management models and solutions of lithium-ion batteries for the development of pure electric vehicles. Renewable and Sustainable Energy Reviews, 64, 106-128. https://doi.org/10.1016/j.rser.2016.05.033

Warner, J. (2015a). Chapter 1 - Introduction. In J. Warner (Ed.), The Handbook of Lithium-Ion Battery Pack Design (pp. 1-8). Elsevier. https://doi.org/10.1016/B978-0-12-801456-1.00001-4

Warner, J. (2015b). Chapter 15 - Lithium-Ion Battery Applications. In J. Warner (Ed.), The Handbook of Lithium-Ion Battery Pack Design (pp. 177-209). Elsevier. https://doi.org/10.1016/B978-0-12-801456-1.00015-4

Warner, J. (2015c). Chapter 3 - Basic Terminology. In J. Warner (Ed.), The Handbook of Lithium-Ion Battery Pack Design (pp. 23-33). Elsevier. https://doi.org/10.1016/B978-0-12-801456-1.00003-8

Warner, J. (2015d). Chapter 6 - Computer-Aided Design and Analysis. In J. Warner (Ed.), The Handbook of Lithium-Ion Battery Pack Design (pp. 59-63). Elsevier. https://doi.org/10.1016/B978-0-12-801456-1.00006-3

Warner, J. (2015e). Chapter 7 - Lithium-Ion and Other Cell Chemistries. In J. Warner (Ed.), The Handbook of Lithium-Ion Battery Pack Design (pp. 65-89). Elsevier. https://doi.org/10.1016/B978-0-12-801456-1.00007-5

Warner, J. (2015f). Chapter 8 - Battery Management System Controls. In J. Warner (Ed.), The Handbook of Lithium-Ion Battery Pack Design (pp. 91-101). Elsevier. https://doi.org/10.1016/B978-0-12-801456-1.00008-7

Warner, J. T. (2019a). Chapter 5 - The Cathodes. In J. T. Warner (Ed.), Lithium-Ion Battery Chemistries (pp. 99-114). Elsevier. https://doi.org/10.1016/B978-0-12-814778-8.00005-3

Warner, J. T. (2019b). In Warner J. T. (Ed.), Chapter 6 - The Anodes. Elsevier. https://doi.org/10.1016/B978-0-12-814778-8.00006-5

Wikner, E., & Thiringer, T. (2018). Extending battery lifetime by avoiding high SOC. Applied Sciences, 8(10), 1825.

Wojtyła, S., Klama, P., & Baran, T. (2017). Is 3D printing safe? Analysis of the thermal treatment of thermoplastics: ABS, PLA, PET, and nylon. Journal of Occupational and Environmental Hygiene, 14(6), D80-D85.

Xiong, R., He, H., Guo, H., & Ding, Y. (2011). Modeling for Lithium-Ion Battery used in Electric Vehicles. Procedia Engineering, 15, 2869-2874. 10.1016/j.proeng.2011.08.540

Xu, W., Wang, J., Ding, F., Chen, X., Nasybulin, E., Zhang, Y., & Zhang, J. -. (2014). Lithium metal anodes for rechargeable batteries. Energy and Environmental Science, 7(2), 513-537. 10.1039/c3ee40795k

Yang, Q., Xu, J., Cao, B., & Li, X. (2017). A simplified fractional order impedance model and parameter identification method for lithium-ion batteries. PLoS One, 12(2), e0172424.

Yann Liaw, B., Nagasubramanian, G., Jungst, R. G., & Doughty, D. H. (2004). Modeling of lithium ion cells—A simple equivalent-circuit model approach. Solid State Ionics, 175(1), 835-839. https://doi.org/10.1016/j.ssi.2004.09.049

Yuan, S., Wu, H., & Yin, C. (2013). State of charge estimation using the extended Kalman filter for battery management systems based on the ARX battery model. Energies, 6(1), 444-470.

Zhang, H., Mu, H. W., Zhang, Y., & Han, J. (2014). Calculation and characteristics analysis of lithium ion batteries' internal resistance using HPPC test. Paper presented at the Advanced Materials Research, , 926 915-918.

Zhao, L., Lin, M., & Chen, Y. (2016). Least-squares based coulomb counting method and its application for state-of-charge (SOC) estimation in electric vehicles. International Journal of Energy Research, 40(10), 1389-1399.

Zhao, R. (2018). Overheating Prediction and Management of Lithium-Ion Batteries https://curve.carleton.ca/a5ce62f7-2a13-427a-9cb3-b8e5d37f2517

Zubi, G., Dufo-López, R., Carvalho, M., & Pasaoglu, G. (2018). The lithium-ion battery: State of the art and future perspectives. Renewable and Sustainable Energy Reviews, 89, 292-308. https://doi.org/10.1016/j.rser.2018.03.002

Appendix A – HPPC test Data sorting

```
clear
clc
% % Start of 15C Data
opts = detectImportOptions('second_15C.xls', 'Sheet','sheet1', 'Range', 'A6:T65536',
'PreserveVariableNames', true);
opts.SelectedVariableNames = opts.SelectedVariableNames([3, 4, 5, 6, 8]);
Table11 = readtable('second_15C.xls', opts);
opts = detectImportOptions('second_15C.xls', 'Sheet','sheet2', 'Range', 'A6:T1337',
'PreserveVariableNames', true);
opts.SelectedVariableNames = opts.SelectedVariableNames([3, 4, 5, 6, 8]);
Table12= readtable('second_15C.xls', opts);
Table_1 = [Table11;Table12]
% Table_2{:,1} = (1:51858).';
% Table_2(:,1) = []
Cap_1(1,:) = Table_1.Var3(Table_1.Var6 < -8.2);
Cap_1(2,:) = Table_1.Var4(Table_1.Var6 < -8.2);
Cap_1(3,:) = Table_1.Var5(Table_1.Var6 < -8.2);
Cap_1(4,:) = Table_1.Var6(Table_1.Var6 < -8.2);
Cap_1 = Cap_1';
save HPPC_Test_LTO.mat
diff_mat_1 = diff(Cap_1(:,1));
break_pt_1 = [0; find(diff_mat_1 ~= 1);994];
for i = 1:length(break_pt_1)-1
   Dis_pulse_1 {i,1} = Cap_1(break_pt_1(i)+1:break_pt_1(i+1),:);
end
%Dis_pulse([1,3,5,7,9,11,13,15,17,19,21],:)
Dis_pulse_1 = Dis_pulse_1
% % Start of 25C Data
opts = detectImportOptions('second_25C.xls', 'Sheet','sheet1', 'Range', 'A6:T65536',
'PreserveVariableNames', true);
opts.SelectedVariableNames = opts.SelectedVariableNames([3, 4, 5, 6, 8]);
Table21 = readtable('second_25C.xls', opts);
opts = detectImportOptions('second_25C.xls', 'Sheet','sheet2', 'Range', 'A6:T4886',
'PreserveVariableNames', true);
opts.SelectedVariableNames = opts.SelectedVariableNames([3, 4, 5, 6, 8]);
Table22= readtable('second_25C.xls', opts);
Table_2 = [Table21;Table22]
% Table_2{:,1} = (1:51858).';
% Table_2(:,1) = []
Cap_2(1,:) = Table_2.Var3(Table_2.Var6 < -8.2);
Cap_2(2,:) = Table_2.Var4(Table_2.Var6 < -8.2);
Cap_2(3,:) = Table_2.Var5(Table_2.Var6 < -8.2);
Cap_2(4,:) = Table_2.Var6(Table_2.Var6 < -8.2)
```

```
Cap_2 = Cap_2';
save HPPC_Test_LTO.mat
diff_mat_2 = diff(Cap_2(:,1));
break_pt_2 = [0; find(diff_mat_2 ~= 1);995];
for i = 1:length(break_pt_2)-1
   Dis_pulse_2 {i,1} = Cap_2(break_pt_2(i)+1:break_pt_2(i+1),:);
end
%Dis_pulse([1,3,5,7,9,11,13,15,17,19,21],:)
Dis_pulse_2 = Dis_pulse_2
save Dis_pulse_2
% % Start of 25C Data
opts = detectImportOptions('second_35C.xls', 'Sheet','sheet1', 'Range', 'A6:T65536',
'PreserveVariableNames', true);
opts.SelectedVariableNames = opts.SelectedVariableNames([3, 4, 5, 6, 8]);
Table_3 = readtable('second_35C.xls', opts);
% Table_2{:,1} = (1:51858).';
% Table_2(:,1) = []
Cap3(1,:) = Table_3.Var3(Table_3.Var6 < -8.2);
Cap3(2,:) = Table_3.Var4(Table_3.Var6 < -8.2);
Cap3(3,:) = Table_3.Var5(Table_3.Var6 < -8.2);
Cap3(4,:) = Table_3.Var6(Table_3.Var6 < -8.2);
Cap3 = Cap3';
save HPPC_Test_LTO.mat
diff_mat_3 = diff(Cap3(:,1));
break_pt_3 = [0; find(diff_mat_3 ~= 1);995];
for i = 1:length(break_pt_3)-1
   Dis_pulse_3{i,1} = Cap3(break_pt_3(i)+1:break_pt_3(i+1),:);
end
save Dis_pulse_3
opts = detectImportOptions('second_45C.xls', 'Sheet','sheet1', 'Range', 'A6:T65536',
'PreserveVariableNames', true);
opts.SelectedVariableNames = opts.SelectedVariableNames([3, 4, 5, 6, 8]);
Table41 = readtable('second_45C.xls', opts);
opts = detectImportOptions('second_45C.xls', 'Sheet','sheet2', 'Range', 'A6:T1181',
'PreserveVariableNames', true);
opts.SelectedVariableNames = opts.SelectedVariableNames([3, 4, 5, 6, 8]);
Table42= readtable('second_45C.xls', opts);
Table_42 = [Table41;Table42]
% Table_2{:,1} = (1:51858).';
% Table_2(:,1) = []
Cap_4(1,:) = Table_42.Var3(Table_42.Var6 < -8.2);
Cap_4(2,:) = Table_42.Var4(Table_42.Var6 < -8.2);
Cap_4(3,:) = Table_42.Var5(Table_42.Var6 < -8.2);
Cap_4(4,:) = Table_42.Var6(Table_42.Var6 < -8.2);
Cap_4 = Cap_4';
```

```
save HPPC_Test_LTO.mat
diff_mat_4 = diff(Cap_4(:,1));
break_pt_4 = [0; find(diff_mat_4 ~= 1);993];
for i = 1:length(break_pt_4)-1
   Dis_pulse4 {i,1} = Cap_4(break_pt_4(i)+1:break_pt_4(i+1),:);
end
%Dis_pulse([1,3,5,7,9,11,13,15,17,19,21],:)
Dis_pulse_4 = Dis_pulse4
save Dis_pulse_4
clearvars -except Dis_pulse_1 Dis_pulse_2 Dis_pulse_3 Dis_pulse_4
Dis_pulse(:,1) = Dis_pulse_1
Dis_pulse(:,2) = Dis_pulse_2
Dis_pulse(:,3) = Dis_pulse_3
Dis_pulse(:,4) = Dis_pulse_4
```

Appendix B – Parameter estimation 1

```
clear
clc
% % Start of 15C Data
opts = detectImportOptions('HOUR_15C.xls', 'Sheet','sheet1', 'Range', 'A6:T65536',
'PreserveVariableNames', true);
opts.SelectedVariableNames = opts.SelectedVariableNames([3, 4, 5, 6, 8, 17]);
Table_10 = readtable('HOUR_15C.xls', opts);
opts = detectImportOptions('HOUR_15C.xls', 'Sheet','sheet2', 'Range', 'A6:T1881',
'PreserveVariableNames', true);
opts.SelectedVariableNames = opts.SelectedVariableNames([3, 4, 5, 6, 8, 17]);
Table_11 = readtable('HOUR_15C.xls', opts);
Table_12 =[Table_10;Table_11]
OCV1(:,2) = Table_12{strcmp(Table_12{:, 'Var4'}, '1:00:00.000'), 'Var5'};
OCV1(:,1) = Table_12{strcmp(Table_12{:, 'Var4'}, '1:00:00.000'), 'Var3'};
OCV1( ~any(OCV1,2), : ) = [];
OCV1([1, 12],:) = [];
OCV_1 = OCV1',;
save OCV_1.mat
load Dis_pulse_1;
Dis_pulse_1 = Dis_pulse_1';
[m, n] = size(Dis_pulse_1);
Ri1 = cell(m, n);
R11 = Ri1;
R12 = Ri1;
C11 = Ri1;
C12 = Ri1;
OCV_1 = Ri1;
% OCV_long = cell(m, 101);
% SOC_long = linspace(0,1,101);
tou1_init1 = 8;
tou2_init1 = 10;
for i = 1:m
   OCV_1(:,i) = OCV_1(:,2);
  for  j=1:n
      xdata = Dis_pulse_1{i, j}(:,1:2);
      ydata = Dis_pulse_1{i, j}(:,3);
      OCP = ydata(1);
      options = optimoptions('lsqcurvefit');
      Ri_init1 = (ydata(6)-ydata(10))/8.68;
      R1_init1 = (ydata(11)-ydata(41))/8.68;
      R2_init1 = (ydata(42)-ydata(end))/8.68;
      C1_init1 = tou1_init1/R1_init1;
      C2_init1 = tou2_init1/R2_init1;
```

```
        x0 = [Ri_init1, R1_init1, C1_init1, R2_init1, C2_init1];
        lb = x0/100;
        ub = x0*100;
        [x,resnorm] = lsqcurvefit(@myfun,x0,xdata,ydata, lb, ub, options);
        clc;
        Ri1{i,j} = x(1);
        R11{i,j} = x(2);
        C11{i,j} = x(3);
        R12{i,j} = x(4);
        C12{i,j} = x(5);
        OCV_1{i,j} = OCP;
        Ri_est1{i,j} = Ri_init1;
        R1_est1{i,j} = R1_init1;
        R2_est1{i,j} = R2_init1;
        C1_est1{i,j} = C1_init1;
        C2_est1{i,j} = C2_init1;
    end
end
clearvars -except Ri1 R11 R12 C11 C12 OCV_1 *_est1 *_long1
SOC1 = linspace(100,0,11);
Capacity_LUT1 = 3.0746;
 Qe_init1 = 0;
 R1_est1 = fliplr(R1_est1);
 R2_est1 = fliplr(R2_est1);
 Ri_est1 = fliplr(Ri_est1);
 C1_est1 = fliplr(C1_est1);
 C2_est1 = fliplr(C2_est1);
 C11 = fliplr(C11);
 C12 = fliplr(C12);
 OCV_1 = fliplr(OCV_1);
 SOC1 = fliplr(SOC1);
R1_est1 = cell2mat(R1_est1);
OCV_1 = cell2mat(OCV_1);
R2_est1 = cell2mat(R2_est1);
C11 = cell2mat(C11);
C12 = cell2mat(C12);
Ri_est1 = cell2mat(Ri_est1);
C1_est1 = cell2mat(C1_est1);
C2_est1 = cell2mat(C2_est1);
opts = detectImportOptions('second_15C.xls', 'Sheet','sheet1', 'Range', 'A6:T65531',
'PreserveVariableNames', true);
opts.SelectedVariableNames = opts.SelectedVariableNames([3, 4, 5, 6, 8, 17]);
Table_13 = readtable('second_15C.xls', opts);
opts = detectImportOptions('second_15C.xls', 'Sheet','sheet2', 'Range', 'A6:T881',
'PreserveVariableNames', true);
```

```
opts.SelectedVariableNames = opts.SelectedVariableNames([3, 4, 5, 6, 8, 17]);
Table_14 = readtable('second_15C.xls', opts);
Table_15 = [Table_13;Table_14]
Table_15 = rmmissing(Table_15,'DataVariables',{'Var3'})
voltage1 = Table_15.Var5(Table_15.Var5 < 2.7)
current1 = Table_15.Var6(Table_15.Var6 < 9)
current1([1],:) = [];
time1 = linspace(1,66331,66331);
time1 = time1';
save fitdata1.mat
% % Start of 25C Data
opts = detectImportOptions('HOUR_25C.xls', 'Sheet','sheet1', 'Range', 'A6:T65536',
'PreserveVariableNames', true);
opts.SelectedVariableNames = opts.SelectedVariableNames([3, 4, 5, 6, 8, 17]);
Table_20 = readtable('HOUR_25C.xls', opts);
opts = detectImportOptions('HOUR_25C.xls', 'Sheet','sheet2', 'Range', 'A6:T4886',
'PreserveVariableNames', true);
opts.SelectedVariableNames = opts.SelectedVariableNames([3, 4, 5, 6, 8, 17]);
Table_21 = readtable('HOUR_25C.xls', opts);
Table_22 = [Table_20;Table_21];
OCV_2 = Table_22{strcmp(Table_22{:, 'Var4'}, '1:00:00.000'), 'Var5'};
OCV_2( ~any(OCV_2,2), : ) = [];
OCV_2([1,2,3,4, 16],:) = [];
OCV_2 = OCV_2',;
save OCV_2.mat
load Dis_pulse_2;
Dis_pulse_2 = Dis_pulse_2';
[m, n] = size(Dis_pulse_2);
Ri2 = cell(m, n);
R21 = Ri2;
R22 = Ri2;
C21 = Ri2;
C22 = Ri2;
OCV_2 = Ri2;
% OCV_long = cell(m, 101);
% SOC_long = linspace(0,1,101);
tou1_init2= 8;
tou2_init2 = 10;
for i = 1:m
   OCV_2(:,i) = OCV_2(:,2);
  for  j=1:n
      xdata = Dis_pulse_2{i, j}(:,1:2);
      ydata = Dis_pulse_2{i, j}(:,3);
      OCP = ydata(1);
      options = optimoptions('lsqcurvefit');
```

```
        Ri_init2 = (ydata(6)-ydata(10))/8.68;
        R1_init2 = (ydata(11)-ydata(41))/8.68;
        R2_init2 = (ydata(42)-ydata(end))/8.68;
        C1_init2 = tou1_init2/R1_init2;
        C2_init2 = tou2_init2/R2_init2;
        x = [Ri_init2, R1_init2, C1_init2, R2_init2, C2_init2];
        lb = x/100;
        ub = x*100;
        [x,resnorm] = lsqcurvefit(@myfun,x,xdata, ydata, lb, ub, options);
        clc;
        Ri2{i,j} = x(1);
        R21{i,j} = x(2);
        C21{i,j} = x(3);
        R22{i,j} = x(4);
        C22{i,j} = x(5);
        OCV_2{i,j} = OCP;
        Ri_est2{i,j} = Ri_init2;
        R1_est2{i,j} = R1_init2;
        R2_est2{i,j} = R2_init2;
        C1_est2{i,j} = C1_init2;
        C2_est2{i,j} = C2_init2;
    end
end
clearvars -except Ri2 R21 R22 C21 C22 OCV_2 *_est2 *_long2
SOC2 = linspace(100,0,11);
Capacity_LUT2 = 3.0746;
Qe_init2 = 0;
 R1_est2 = fliplr(R1_est2);
 R2_est2 = fliplr(R2_est2);
 Ri_est2 = fliplr(Ri_est2);
 C1_est2 = fliplr(C1_est2);
 C2_est2 = fliplr(C2_est2);
 C21 = fliplr(C21);
 C22 = fliplr(C22);
 OCV_2 = fliplr(OCV_2);
 SOC2 = fliplr(SOC2);
R1_est2 = cell2mat(R1_est2);
OCV_2 = cell2mat(OCV_2);
R2_est2 = cell2mat(R2_est2);
C21 = cell2mat(C21);
C22 = cell2mat(C22);
Ri_est2 = cell2mat(Ri_est2);
C1_est2 = cell2mat(C1_est2);
C2_est2 = cell2mat(C2_est2);
```

```
opts = detectImportOptions('second_25C.xls', 'Sheet','sheet1', 'Range', 'A6:T65531',
'PreserveVariableNames', true);
opts.SelectedVariableNames = opts.SelectedVariableNames([3, 4, 5, 6, 8, 17]);
Table_21 = readtable('second_25C.xls', opts);
Table_21 = rmmissing(Table_21,'DataVariables',{'Var3'});
voltage2 = Table_21.Var5(Table_21.Var5 < 2.7)
current2 = Table_21.Var6(Table_21.Var6 < 9)
current2(1,:) = [];
time2 = linspace(1,65459,65459);
time2 = time2';
save fitdata2.mat;
% % Start of 35C Data
opts = detectImportOptions('HOUR_35C.xls', 'Sheet','sheet1', 'Range', 'A6:T65536',
'PreserveVariableNames', true);
opts.SelectedVariableNames = opts.SelectedVariableNames([3, 4, 5, 6, 8, 17]);
Table_30 = readtable('HOUR_35C.xls', opts);
OCV_3 = Table_30{strcmp(Table_30{:, 'Var4'}, '1:00:00.000'), 'Var5'};
OCV_3( ~any(OCV_3,2), : ) = [];
OCV_3([1, 12],:) = [];
OCV_3 = OCV_3',;
save OCV_3.mat
load Dis_pulse_3;
Dis_pulse_3 = Dis_pulse_3';
[m, n] = size(Dis_pulse_3);
Ri3 = cell(m, n);
R31 = Ri3;
R32 = Ri3;
C31 = Ri3;
C32 = Ri3;
OCV_3 = Ri3;
% OCV_long = cell(m, 101);
% SOC_long = linspace(0,1,101);
tou1_init3= 8;
tou2_init3 = 10;
for i = 1:m
   OCV_3(:,i) = OCV_3(:,2);
  for  j=1:n
      xdata = Dis_pulse_3{i, j}(:,1:2);
      ydata = Dis_pulse_3{i, j}(:,3);
      OCP = ydata(1);
      options = optimoptions('lsqcurvefit');
      Ri_init3 = (ydata(6)-ydata(10))/8.68;
      R1_init3 = (ydata(11)-ydata(41))/8.68;
      R2_init3 = (ydata(42)-ydata(end))/8.68;
      C1_init3 = tou1_init3/R1_init3;
```

```
        C2_init3 = tou2_init3/R2_init3;
        x = [Ri_init3, R1_init3, C1_init3, R2_init3, C2_init3];
        lb = x/100;
        ub = x*100;
        [x,resnorm] = lsqcurvefit(@myfun,x,xdata, ydata, lb, ub, options);
        clc;
        Ri3{i,j} = x(1);
        R31{i,j} = x(2);
        C31{i,j} = x(3);
        R32{i,j} = x(4);
        C32{i,j} = x(5);
        OCV_3{i,j} = OCP;
        Ri_est3{i,j} = Ri_init3;
        R1_est3{i,j} = R1_init3;
        R2_est3{i,j} = R2_init3;
        C1_est3{i,j} = C1_init3;
        C2_est3{i,j} = C2_init3;
    end
end
clearvars -except Ri3 R31 R32 C31 C32 OCV_3 *_est3 *_long3
SOC3 = linspace(100,0,11);
Capacity_LUT3 = 3.0746;
Qe_init3 = 0;
 R1_est3 = fliplr(R1_est3);
 R2_est3 = fliplr(R2_est3);
 Ri_est3 = fliplr(Ri_est3);
 C1_est3 = fliplr(C1_est3);
 C2_est3 = fliplr(C2_est3);
 C31 = fliplr(C31);
 C32 = fliplr(C32);
 OCV_3 = fliplr(OCV_3);
 SOC3 = fliplr(SOC3)
R1_est3 = cell2mat(R1_est3);
OCV_3 = cell2mat(OCV_3);
R2_est3 = cell2mat(R2_est3);
C31 = cell2mat(C31);
C32 = cell2mat(C32);
Ri_est3 = cell2mat(Ri_est3);
C1_est3 = cell2mat(C1_est3);
C2_est3 = cell2mat(C2_est3);
opts = detectImportOptions('second_35C.xls', 'Sheet','sheet1', 'Range', 'A6:T65531',
'PreserveVariableNames', true);
opts.SelectedVariableNames = opts.SelectedVariableNames([3, 4, 5, 6, 8, 17]);
Table_31 = readtable('second_35C.xls', opts);
Table_31 = rmmissing(Table_31,'DataVariables',{'Var3'});
```

```
voltage3 = Table_31.Var5(Table_31.Var5 < 2.7)
current3 = Table_31.Var6(Table_31.Var6 < 9)
time3 = linspace(1,44130,44130);
time3 = time3';
save fitdata3.mat;
% % % % %  Start of 45c Data
opts = detectImportOptions('HOUR_45C.xls', 'Sheet','sheet1', 'Range', 'A6:T65536',
'PreserveVariableNames', true);
opts.SelectedVariableNames = opts.SelectedVariableNames([3, 4, 5, 6, 8, 17]);
Table_40 = readtable('HOUR_45C.xls', opts);
opts = detectImportOptions('HOUR_25C.xls', 'Sheet','sheet2', 'Range', 'A6:T881',
'PreserveVariableNames', true);
opts.SelectedVariableNames = opts.SelectedVariableNames([3, 4, 5, 6, 8, 17]);
Table_41 = readtable('HOUR_45C.xls', opts);
Table_42 =[Table_40;Table_41]
OCV4(:,2) = Table_42{strcmp(Table_42{:, 'Var4'}, '1:00:00.000'), 'Var5'};
OCV4(:,1) = Table_42{strcmp(Table_42{:, 'Var4'}, '1:00:00.000'), 'Var3'};
OCV4( ~any(OCV4,2), : ) = [];
OCV4([1, 12],:) = [];
OCV_4 = OCV4',;
save OCV_4.mat
load Dis_pulse_4;
Dis_pulse_4 = Dis_pulse_4';
[m, n] = size(Dis_pulse_4);
Ri4 = cell(m, n);
R41 = Ri4;
R42 = Ri4;
C41 = Ri4;
C42 = Ri4;
OCV_4 = Ri4;
% OCV_long = cell(m, 101);
% SOC_long = linspace(0,1,101);
tou1_init4 = 8;
tou2_init4 = 10;
for i = 1:m
   OCV_4(:,i) = OCV_4(:,2);
  for  j=1:n
      xdata = Dis_pulse_4{i, j}(:,1:2);
      ydata = Dis_pulse_4{i, j}(:,3);
      OCP = ydata(1);
      options = optimoptions('lsqcurvefit');
      Ri_init4 = (ydata(6)-ydata(10))/8.68;
      R1_init4 = (ydata(11)-ydata(41))/8.68;
      R2_init4 = (ydata(42)-ydata(end))/8.68;
      C1_init4 = tou1_init4/R1_init4;
```

```
        C2_init4 = tou2_init4/R2_init4;
        x0 = [Ri_init4, R1_init4, C1_init4, R2_init4, C2_init4];
        lb = x0/100;
        ub = x0*100;
        [x,resnorm] = lsqcurvefit(@myfun,x0,xdata,ydata, lb, ub, options);
        clc;
        Ri4{i,j} = x(1);
        R41{i,j} = x(2);
        C41{i,j} = x(3);
        R42{i,j} = x(4);
        C42{i,j} = x(5);
        OCV_4{i,j} = OCP;
        Ri_est4{i,j} = Ri_init4;
        R1_est4{i,j} = R1_init4;
        R2_est4{i,j} = R2_init4;
        C1_est4{i,j} = C1_init4;
        C2_est4{i,j} = C2_init4;
    end
end
clearvars -except Ri4 R41 R42 C41 C42 OCV_4 *_est4 *_long4
SOC4 = linspace(100,0,11);
Capacity_LUT4 = 3.0746;
Qe_init4 = 0;
 R1_est4 = fliplr(R1_est4);
 R2_est4 = fliplr(R2_est4);
 Ri_est4 = fliplr(Ri_est4);
 C1_est4 = fliplr(C1_est4);
 C2_est4 = fliplr(C2_est4);
 C41 = fliplr(C41);
 C42 = fliplr(C42);
 OCV_4 = fliplr(OCV_4);
 SOC4 = fliplr(SOC4);
R1_est4 = cell2mat(R1_est4);
OCV_4 = cell2mat(OCV_4);
R2_est4 = cell2mat(R2_est4);
C41 = cell2mat(C41);
C42 = cell2mat(C42);
Ri_est4 = cell2mat(Ri_est4);
C1_est4 = cell2mat(C1_est4);
C2_est4 = cell2mat(C2_est4);
opts = detectImportOptions('second_45C.xls', 'Sheet','sheet1', 'Range', 'A6:T65531',
'PreserveVariableNames', true);
opts.SelectedVariableNames = opts.SelectedVariableNames([3, 4, 5, 6, 8, 17]);
Table_43 = readtable('second_45C.xls', opts);
```

```
opts = detectImportOptions('second_45C.xls', 'Sheet','sheet2', 'Range', 'A6:T881',
'PreserveVariableNames', true);
opts.SelectedVariableNames = opts.SelectedVariableNames([3, 4, 5, 6, 8, 17]);
Table_44 = readtable('second_45C.xls', opts);
Table_45 = [Table_43;Table_44]
Table_45 = rmmissing(Table_45,'DataVariables',{'Var3'})
voltage4 = Table_45.Var5(Table_45.Var5 < 2.7)
current4= Table_45.Var6(Table_45.Var6 < 9)
current4([1],:) = [];
time4 = linspace(1,54476,54476);
time4 = time4'
save fitdata4.mat
clearvars -except fitdata1 fitdata2 fitdata3 fitdata4
```

Appendix C – Parameter estimation 2

```
clear
clc
load fitdata1.mat
load fitdata2.mat
load fitdata3.mat
load fitdata4.mat
Temperature_LUT(1,:) = [288 298 308 318];
%  Temperature_LUT = Temperature_LUT';
%
SOC(1,:) = SOC1
SOC(2,:) = SOC2
SOC(3,:) = SOC3
SOC(4,:) = SOC4
SOC = SOC';
OCV(1,:) = OCV_1
OCV(2,:) = OCV_2
OCV(3,:) = OCV_3
OCV(4,:) = OCV_4
OCV= OCV';
Ri(1,:) = Ri1
Ri(2,:) = Ri2
Ri(3,:) = Ri3
Ri(4,:) = Ri4
Ri = Ri';
Ri_est(1,:) = Ri_est1
Ri_est(2,:) = Ri_est2
Ri_est(3,:) = Ri_est3
Ri_est(4,:) = Ri_est4
Ri_est = Ri_est'
R1(1,:) = R11
R1(2,:) = R21
R1(3,:) = R31
R1(4,:) = R41
R1 = R1';
R1_est(1,:) = R1_est1
R1_est(2,:) = R1_est2
R1_est(3,:) = R1_est3
R1_est(4,:) = R1_est4
R1_est = R1_est';
R2(1,:) = R12
R2(2,:) = R22
R2(3,:) = R32
R2(4,:) = R42
R2 = R2';
R2_est(1,:) = R2_est1
R2_est(2,:) = R2_est2
```

```
R2_est(3,:) = R2_est3
R2_est(4,:) = R2_est4
R2_est = R2_est';
C1(1,:) = C11
C1(2,:) = C21
C1(3,:) = C31
C1(4,:) = C41
C1 = C1';
C1_est(1,:) = C1_est1
C1_est(2,:) = C1_est2
C1_est(3,:) = C1_est3
C1_est(4,:) = C1_est4
C1_est = C1_est';
C2(1,:) = C12
C2(2,:) = C22
C2(3,:) = C32
C2(4,:) = C42
C2 = C2';
C2_est(1,:) = C2_est1
C2_est(2,:) = C2_est2
C2_est(3,:) = C2_est3
C2_est(4,:) = C2_est4
C2_est = C2_est';
Capacity_LUT(1,:) = Capacity_LUT1
Capacity_LUT(2,:) = Capacity_LUT2
Capacity_LUT(3,:) = Capacity_LUT3
Capacity_LUT(4,:) = Capacity_LUT4
Capacity_LUT = Capacity_LUT';
Qe_init = 0
voltage(1,:) = voltage1;
current(1,:) = current1;
time(1,:) = time1;
clearvars -except voltage current time R1_est Ri_est R2_est C1_est C2_est
Capacity_LUT1 Capacity_LUT Qe_init SOC SOC1 SOC2 SOC3 SOC4 OCV
Temperature_LUT R1 R2 C1 C2
save Parameter_estimation_Data
```